EFFECT OF RIPENING STAGES AND SHAPES OF BANANA SLICES ON TEMPERATURE PROFILES PREDICTION DURING MICROWAVE HEATING

WISARA THUTO

A THESIS SUBMITTED IN PARTIAL FULFILLMENT OF

THE REQUIREMENT FOR THE DEGREE OF DOCTOR OF PHILOSOPHY

IN FOOD SCIENCE

SCHOOL OF FOOD INDUSTRY

KING MONGKUT'S INSTITUTE OF TECHNOLOGY LADKRABANG

2021

KMITL-2021-FI-D-051-394

Thesis Title	Effect of ripening stages and shapes of banana slices on temperature profiles prediction during microwave heating
Student	Miss Wisara Thuto
Student ID	63608002
Degree	Doctor of Philosophy
Program	Food Science (International Program)
Year	2021
Thesis Adviser	Dr. Kittichai Banjong

ABSTRACT

The finite element method was used to study the effect of ripening stages and shapes of banana slices on temperature profiles prediction during microwave heating. COMSOL multiphysics software was employed to perform the simulation task. The simulation results were validated with experimental data. The dehydration phenomenon of banana slices are examined. The profiles of temperature, moisture, vapor pressure are discussed. Both ripening stages and shapes of banana slices lead to non-uniform temperature distribution. More heat generation was observed around the center region of the banana slices. Heat and moisture were transported from the center of the banana slices to its surface. At the center of the banana slices, the temperature increased rapidly and reached its highest temperature with the negative temperature gradient toward the boundary surface. A higher heat flux was observed from the beginning period along with the increasing time steps until 50 s. Heat generation decreased during 50 s to 60 s, coinciding with a small rise in temperature, but the temperature gradient remained constant. The water convective flux peaked around 11 mm from the center. The vapor pressure peaked at the center for all cases.

ACKNOWLEDGEMENTS

I would like to express my deepest appreciation to my thesis advisor, Dr. Kittichai Banjong for his guidance, not only the research methodologies but also many other methodologies in life. I would not have achieved this far, and this thesis would not have been completed without all the support that I have always received from his.

I acknowledge my heartfelt thanks to Asst. Prof. Dr. Soraya Kerdpiboon, Chairperson of Ph.D. Program in Food Science (International Program), KMITL, for her advice and assistance in keeping my progress on schedule.

I would like to extend my sincere thanks to the thesis committees for their valuable advising, suggesting, and reviewing my thesis.

I am also very grateful to all staffs at the School of Food Industry, KMITL, especially Mrs. Siriporn Tankaew, who was always so helpful and provided me with her assistance throughout my thesis.

Finally, but most of all, I would like to express my deepest gratitude to my belove mother, Mrs. Winithorn Thuto, my supportive aunt, Ms. Feung Boonnop and Mr. Dachdanai Boonchauy for their love, ceaseless care, understanding and encouragement during my whole life.

Wisara Thuto

CONTENTS

Page

CONTENTS (Cont'd)

Page

CONTENTS (Cont'd)

Page

CONTENTS (Cont'd)

Page

LIST OF TABLES

Page

LIST OF FIGURES

Page

LIST OF FIGURES (Cont'd)

Page

LIST OF ABBREVIATIONS

FEM	Finite element method
FEA	Finite element analysis
FE	Finite element
EM model	Electromagnetic field analysis model
HT model	Heat transfer analysis model
REV	Representative elementary volume
CSIRO	Commonwealth Scientific and Industrial Research Organisation
PDE	Partial differential equation
TE	Transverse electric
TM	Transverse magnetic
CAD	Computer-Aided Design
ASG	Analysis suitable geometry

NOMENCLATURE

E	Electric field intensity (V/m)
H	Magnetic field intensity (A/m)
ω	Angular frequency (rad/s)
ε_0	Permittivity of free space (8.854×10^{-12} F/m)
j	Complex number operator
ε	Complex relative permittivity
ε'	Dielectric constant
ε''	Dielectric loss factor
μ_r	Relative permeability of the food material
ε_r	Relative permittivity
k_0	Wave number
σ	Electrical conductivity (S/m)
Q_m	Heat generation due to microwaves (W/m^3)
f	Frequency (Hz)
ΔV	Representative elementary volume (m^3)
ΔV_g	Volume of gas (m^3)
ΔV_w	Volume of water (m^3)
ΔV_s	Volume of solid (m^3)
φ	Equivalent porosity
S_w	Equivalent saturation of water
S_g	Equivalent saturation of gas
ρ_v	Mass density of vapor (kg/m^3)
ρ_a	Mass density of air (kg/m^3)
ρ_g	Mass density of gas (kg/m^3)
p_v	Partial pressure of vapor (Pa)
p_a	Partial pressure of air (Pa)
P	Total pressure (Pa)

NOMENCLATURE (Cont'd)

M_v	Molar mass of vapor (kg/mol)
M_a	Molar mass of air (kg/mol)
M_g	Molar mass of gas (kg/mol)
Δm_v	Mass of vapor in a representative elementary volume (kg)
Δm_a	Mass of air in a representative elementary volume (kg)
R	Universal gas constant (J/mol K)
T	Temperature (K)
c_v	Mass concentration of vapor (kg/m^3)
c_a	Mass concentration of air (kg/m^3)
c_w	Mass concentration of liquid water (kg/m^3)
Δm_w	Mass of liquid water in a representative elementary volume (kg)
ρ_w	Density of water (kg/m^3)
k_w	Intrinsic permeability of water (m^2)
$k_{r,w}$	Relative permeability of water
μ_w	Viscosity of water (Pa s)
D_c	Capillary diffusivity (m^2/s)
R_{evap}	Evaporation rate of liquid water to water vapor (kg/m^2 s)
ω_v	Mass fraction of vapor
k_g	Intrinsic permeability of gas (m^2)
$k_{r,g}$	Relative permeability of gas
μ_g	Viscosity of gas (Pa s)
$D_{eff,g}$	Binary diffusivity of vapor and air (m^2/s)
ω_a	Mass fraction of air
$\vec{n}_w$	Water flux (kg/m^2 s)
$\vec{n}_g$	Gas flux (kg/m^2 s)
h_g	Enthalpy of gas (J)
h_w	Enthalpy of water (J)

NOMENCLATURE (Cont'd)

h_{fg}	Latent heat of evaporation (J/kg)
ρ_{eff}	Effective density (kg/m^3)
c_{peff}	Effective specific heat (J/kg K)
k_{eff}	Effective thermal conductivity (W/m K)
ρ_s	Solid density (kg/m^3)
c_{pg}	Specific heat capacity of gas (J/kg K)
c_{pw}	Specific heat capacity of water (J/kg K)
c_{ps}	Specific heat capacity of solid (J/kg K)
$k_{th,g}$	Thermal conductivity of gas (W/m K)
$k_{th,w}$	Thermal conductivity of water (W/m K)
$k_{th,s}$	Thermal conductivity of solid (W/m K)
m_g	Mass fraction of gas (kg)
m_w	Mass fraction of water (kg)
m_s	Mass fraction of solid (kg)
K_{evap}	Evaporation constant (1/s)
$p_{v,eq}$	Equilibrium vapor pressure (Pa)
$\vec{n}_{w,s}$	Total water flux at the surface (kg/m^2 s)
$\vec{n}_{v,s}$	Total vapor flux at the surface (kg/m^2 s)
h_{mv}	Mass transfer coefficient (m/s)
$p_{v,air}$	Vapor pressure of ambient air (Pa)
P_{amb}	Ambient pressure (Pa)
h_T	Heat transfer coefficient (W/m2K)
T_{air}	Drying air temperature (K)
C_v	Specific heat of vapor at constant volume (J/kg K)
d_p	Penetration depth in the material (mm)
λ	Wavelength (m)
$tan\,\delta$	Dielectric loss tangent

CHAPTER 1

INTRODUCTION

1.1 Introduction

Bananas are a climacteric fruit grown commercially in many tropical countries (Maskan, 2000; Zotarelli et al., 2012). Bananas are highly nutritious, and ripening is an indispensable process for the development of the nutritional aspects of a banana. The physical and chemical properties of bananas change at the different stages of ripening. When a banana starts to ripen, carbohydrates are initially present in the form of starches but then they transform into sugars, which are major soluble solids. Therefore, unripe bananas taste starchy and bland, or less sweet, while ripe bananas taste sweet (Huang, 2013; Siriboon & Banlusilp, 2004). Bananas are well suited to industrial processing due to their rich content of soluble solids and minerals and their low acidity (Pragati et al., 2014). Bananas can be consumed raw, cooked or processed into many types of food products (Pisutpaisal et al., 2014). In addition to preserving bananas, dehydration through many different processes has been reported by researchers (such as solar drying, convective air drying, osmotic dehydration, frying, vacuum drying, freeze drying, etc.), indicating the importance of this widely-appreciated tropical fruit (Monteiro et al., 2016).

Dehydration is a common method and a widely used means of food preservation, since the removal of moisture prevents the growth and reproduction of micro-organisms, enzymatic activity, and chemical reactions, thereby extending the shelf life of the food and reducing the transportation and storage costs (Malafronte et al., 2012; Zotarelli et al., 2012; Monteiro et al., 2016). Among the numerous dehydration methods available, microwave heating has gained popularity as an alternative dehydration technique. Microwave heating is known for its benefits, such as its ability to achieve high heating rates, reduction in treatment time, and minimal changes to the flavor, color, and nutritional qualities of the food. There are also advantages in terms of environmental impact; microwave heating saves more energy when compared with conventional heating methods, and therefore has a reduced impact on the environment (Geedipalli et al., 2007; Campañone et al., 2014; Chandrasekaran et al., 2013). When food is heated in a microwave, its heat is able to reach the center of the food, whereupon the electromagnetic radiation

is absorbed by dipolar molecules which occur in fat or water, thereby allowing heat to be generated. Kinetic energy is generated by the microwave radiation, causing the vibration of water molecules, which in turn creates friction. This heats the water and leads to evaporation. As a consequence, significant vapor pressure differences arise between the surface of the food and its core, which allows the moisture to be drawn out of the food item (Barba & d'Amore, 2012; Chandrasekaran et al., 2013). Microwave heating characteristics are affected by many factors; a review of microwave food processing was published showing that many interacting factors influence the temperature distribution in heated food during the microwave heating process, such as dielectric properties, physical properties, and thermal properties of the foods and heating conditions (Chandrasekaran et al., 2013; Houšová & Hoke, 2001; Liu et al., 2014; Pitchai et al., 2014). The complexity of the influence of these factors on temperature distribution during microwave heating presents a serious problem (Houšová & Hoke, 2001); these factors affect microwave heating uniformity and can thus produce a non-uniform temperature distribution within the food (Pitchai et al., 2014). Non-uniform temperature distribution is the source of many problems (Basak & Meenakshi, 2006; Liu et al., 2014), such as the creation of hot spots and cold spots (Zhang et al., 2018), which can seriously affect the quality of the food (Geedipalli et al., 2007; Zhang et al., 2018). Around the location of hot spots, the temperature may be too high and can damage the nutrient substance or can cause burns or quality degradation of the final products (Zhu et al., 2018). Meanwhile, around the cold spots as well as undercooked areas, the low temperature may fail to reach the necessary level to eliminate microorganisms, which raises the risk of food deterioration and foodborne illnesses (Liu et al., 2014; Zhu et al., 2018).

Experimental measurements of temperatures in a microwave oven during heating are limited due to the interference of measuring devices and the continuous nature of the process (Salvi et al., 2011), which causes the temperature distribution in food materials to be very difficult to monitor and predict. This lack of information makes it difficult to determine the optimal process and to control the safety of food products. Computer simulation has been suggested as one of the best ways to understand complex microwave heating (Resurreccion Jr et al., 2013; Boz et al., 2014; Liu et al., 2014); its process consists of creating geometry, forming the computational geometry with a mesh, and then solving the governing equations with a suitable numerical method (Boz et al., 2014), such as the Finite Difference Method (FDM), Finite Volume Method (FVM), Finite Element Method (FEM) or Boundary Element Method

(BEM), etc. In order to simulate the microwave heating process, various researchers have used the FEM to examine the microwave heating process in food due to its characteristic ability to handle irregular shapes and material properties (Pandit & Prasad, 2003; Martins, 2006; Liu et al., 2013; Song et al., 2018). The ability to use a simulation eliminates the need to perform multiple experiments. There is no need to replicate conditions, and the process is speeded up immeasurably. This allows research to be carried out quickly and at minimal cost (Martins, 2006; Song et al., 2018). However, the difficult stage in the simulation is the use of independent numerical codes that are highly complex in geometry generation, equation solving, and results visualization. Accordingly, programming and numerical analysis skills are required (Salvi et al., 2011).

While numerous studies have been carried out involving computer simulations to investigate the characteristics of food materials affected by different drying methods (Ranjan et al., 2004; Karim & Hawlader, 2005; Swasdisevi et al., 2007; Doymaz, 2010; Monteiro et al., 2016;), there has been no studies on the effect of ripening stages and shapes of banana on temperature profiles during microwave heating. Additionally, research to date has not provided significant insights into the processes involved from a physical perspective. Among these studies, it is assumed that energy involves conductive heat transfer, while moisture involves diffusive transport, but an accurate understanding of the mechanisms underpinning the transport process when microwaves are used for heating has not yet been achieved (Pitchai et al., 2014). To resolve this lack of understanding, it is necessary to establish a model which can couple heat and mass transfer to make predictions for the distribution of moisture and the temperature within the material undergoing dehydration (Kumar et al., 2016). Understanding these effects and various forms of behavior could be beneficial for the improvement, development, and design of optimum processes for dehydration in bananas with a microwave or microwave-assisted heating.

Such discussions aim at improving the understanding the effect of ripening stages and shapes on temperature profiles and investigate the phenomena of heat and moisture transport in bananas during microwave heating process based on finite element model.

1.2 Objectives

The specific objectives of this study were:

1.2.1 To establish a FE model to study the temperature profiles of banana slices during microwave heating process.

1.2.2 To demonstrate the effect of ripening stages of banana slices on temperature profiles during microwave heating process based on FE model.

1.2.3 To demonstrate the effect of shapes of banana slices on temperature profiles during microwave heating process based on FE model.

1.2.4 To investigate the phenomena of heat and moisture transport in banana slices during microwave heating process based on FE model.

1.3 Scope of research

The main scopes of this study were:

1.3.1 The local cultivated banana cv. 'Kluai Namwa' (*Musa sapientum* Linn., ABB group) was used as banana samples to study the effects of two ripening stages: unripe and ripe bananas and two different shapes: transversal and longitudinal on temperature profiles and investigate the phenomena of heat and moisture transport during microwave heating.

1.3.2 Banana samples were treated with 800 W microwave at an excitation frequency of 2.45 GHz, the TE_{10} mode is the only propagation mode for 60 s.

1.3.3 The FEM was used to establish and apply for simulating a 3-Dimension model through the COMSOL multiphysics software.

1.3.4 The simulated models were validated with the experimental measurements.

CHAPTER 2

LITERATURE REVIEW

2.1 Banana

2.1.1 Banana general background

Bananas are perennial herbaceous plants and belongs to the family Musaceae (Arvanitoyannis et al., 2008). There are a lot of species of bananas, different kind of bananas differ for size, taste and flesh structure that can be more or less firm. Additionally, there is a giant herbaceous plant similar to the banana tree, called plantain. Its fruit is larger and thicker with harder skin, compared with the banana. Most edible bananas and plantains are seedless and sterile with an asexual propagation. These edible bananas are the main fruit in international fruit and vegetable market (Arvanitoyannis et al., 2008).

In general, Southeast Asia is recognized center of origin of bananas. Banana is a climateric fruit cultivated in numerous countries throughout the tropical and subtropical regions. The main producers of banana are Asia, Latin America and Africa, such as India, China, Philippines, Ecuador and Brazil (Bello-Pérez et al., 2011).

Banana is a nutritious fruit, a good source of fiber, potassium, vitamins, antioxidants and phytonutrients (Lahav, 1995). The nutritional content based on cultivars, the conditions at the planting sites, and the ripening stage of the fruit (Thaiphanit & Anprung, 2010; Youryon & Supapvanich, 2016). It can be eaten either raw as a fruit or cooked as a delicious dish. Commonly, ripe bananas are consumed raw while unripe bananas are used as a cooking ingredient due to their high starch and fiber content (Aurore et al., 2009).

Besides being a promising food source to satisfy the nutritional requirements of the local, bananas are one of the important traded fruits in the world. The banana trade plays an important role in the economy of exporting countries, provides job opportunities, improves economies, and increases incomes (Raynolds, 2003; Ruben & van Schendel, 2008).

2.1.2 Cultivated banana

Cultivated bananas are referred to *Musa* spp., their major genomic groups are mostly combined between the A and B genomes, which inherited from *Musa acuminata* Colla. and *Musa balbisiana* Colla. (Brown et al., 2009). Most cultivated bananas are classified into diploids (AA, AB and BB) and triploids (AAA, AAB, ABB and BBB) genomic groups (Pillay et al., 2004).

In Thailand, the local cultivated banana cv. 'Kluai Namwa' (*Musa sapientum* Linn., ABB group) has been domestically planted throughout Thailand (Jaiturong et al., 2020a, 2020b), the fruits are usually elongate, cylindrical, and slightly curved at the ends with thin or thick skin and peel color ranging from green to yellow during ripening (Figure 2.1) (Ghag & Ganapathi, 2019).

Kluai Namwa is economically important for both domestic consumption and export (Vatanasuchart et al., 2015). Additionally, Kluai Namwa is high in starch content at the green stage, and high in non-starch polysaccharides (e.g. pectin, cellulose and hemicelluloses) at fully yellow stage thus both ripe and unripe Kluai Namwa are suitable for food applications (Duan et al., 2008; Siriboon & Banlusilp, 2004; Vatanasuchart et al., 2015; Vatanasuchart et al., 2012). The nutritional components within the flesh of its unripe and ripe fruits were roughly determined as shown in Table 2.1.

Figure 2.1 Photographs of banana (Kluai Namwa) fruit at different ripening stages.
Source: Vatanasuchart et al. (2012)

Table 2.1 Nutritional composition of unripe and ripe Kluai Namwa banana fruits. (per 100 g)

Composition	Unit	Unripe	Ripe
Moisture	%	69.00	71.60
Energy	Cal	110.00	100.00
Fat	g	0.20	0.30
Carbohydrate	g	28.70	26.10
Protein	g	1.40	1.20
Calcium	mg	8.00	12.00
Phosphorus	mg	35.00	32.00
Iron	mg	0.90	0.80
Vitamin A	IU	483.00	375.00
Vitamin B1	mg	0.04	0.03
Vitamin B2	mg	0.02	0.04
Vitamin B3	mg	0.60	0.60
Vitamin C	mg	31.00	14.00

Source: Panyakham et al. (2014)

2.1.3 Changes during ripening of bananas

The ripening process includes several noticeable changes that take place simultaneously (Siriboon & Banlusilp, 2004). Inedible mature banana fruit transforms into edible banana fruit by ripening process (Wills & Golding, 2016). The changes of banana fruit during ripening process are shown in Table 2.2.

2.1.3.1 Color

During the ripening process, the peel changes the color from green to yellow due to chlorophyll degradation, which losses of green color and reveals the yellow carotenoid pigments (Smith et al., 1990; Seymour, 1993; Caussiol, 2001). The whiteness and lightness of the pulp color decreased while the yellowness remained constant during ripening and notably increased at the overripe stage (Wainwright & Hughes, 1990; Youryon & Supapvanich, 2017). The color changing stage is a great indicator for evaluating banana fruit quality (Caussiol, 2001). Based on banana peel color, CSIRO (CSIRO, 1972) provide a banana ripening guide as shown in Table 2.3, and USDA (USDA, 2004) provide a list of degrees of ripeness and a standard color index showing the ripening stages of banana as shown in Table 2.4 and Figure 2.2, respectively, these indexes are widely used in industry.

Table 2.2 The changes which occur during banana ripening.

General changes	Specific changes
Color	Breakdown of chlorophyll in peel (green to yellow)
Texture	Alteration in the composition of cell wall. Increase in tissue permeability (change in water relations of peel and pulp). Softening of pulp (Solubilisation of pectins and hydration of cell walls). Hydrolysis of starch and accumulation of sugars.
Metabolic	Increase in respiration and transpiration rate. Synthesis and evolution of Ethylene (increases just before ripening). Altered regulation of existing metabolic pathways. Changes in fatty acid composition of peel and pulp. Increase and activation of enzymes. Production of protein.
Flavor and aroma	Decrease in active tannins in peel and pulp. Production of volatiles.

Source: Caussiol (2001)

Table 2.3 CSIRO Banana ripening guide.

Stage	Peel color	Observations
1	Green	Hard, rigid, no ripening
Sprung	Green	Bends slightly, ripening started
2	Green-trace of yellow	-
3	More green than yellow	-
4	More yellow than green	-
5	Yellow-Green tip	-
6	Full Yellow	Peels readily, firm ripe
7	Yellow lightly flecked with brown	Fully ripe, aromatic
8	Yellow with increasing brown areas	Overripe, pulp very soft and darkening, highly aromatic

Source: CSIRO (1972)

Table 2.4 USDA List of degrees of banana ripeness.

Stage	Index No.	Peel color
Green	1	Green
	2	Light green, breaking slight toward yellow
Turning Yellow	3	Yellowish-green, more green than yellow
	4	Greenish-yellow, more yellow than green
Ripe	5	Yellow with green tips
	6	Yellow
	7	Yellow, flecked with brown

Source: USDA (2004)

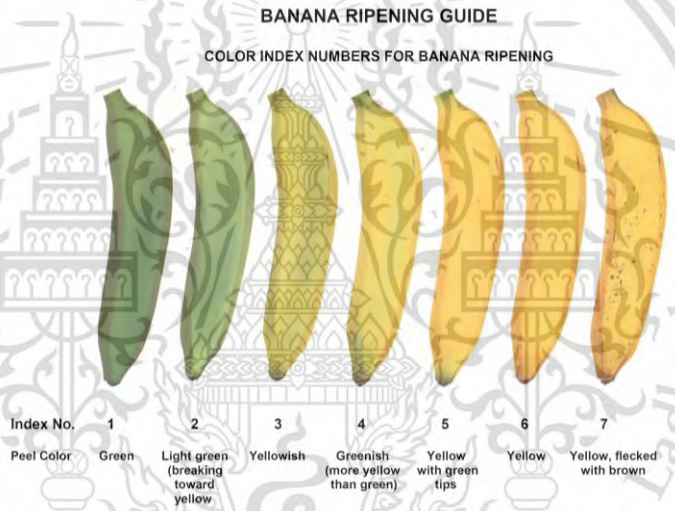

Figure 2.2 USDA Color indexes for banana ripening.
Source: USDA (2004)

2.1.3.2 Texture

It has been shown that the alteration in cell wall structure due to degradation of starch and degrading enzymes such as polyglacteronase caused the banana fruit to soften rapidly (Seymour, 1993; Caussiol, 2001) during the ripening process. In addition, texture of banana fruit shows correlations with a mechanical sense of firmness (Kramer & Twigg, 1962) which used as indicator to evaluate food quality and the stages of ripeness (Abbott, 1999; Soltani et al., 2011).

2.1.3.3 Aroma

The banana contains a mixture of volatile compounds include esters, phenol esters, alcohols (e.g. aldehydes), and carbonyl compounds (e.g. ketones) which are present its characteristic aroma. The synthesis of volatile compounds in banana relative to its ripening stages due to the conversion of starch and texture. Table 2.5 shows the aroma components of banana at different ripening stages (Seymour, 1993).

Table 2.5 The prototypical aromatic compounds of banana fruit.

Banana stage	**Aroma components**
Green	2-Hexaenal
Ripe	Eugenol
Overripe	Isopentanol

Source: Caussiol (2001)

2.1.3.4 Organic acids

It has been shown that at the fully ripe stage, the pH of peel and pulp of banana at harvest is about 5.4 to 6.0 and then decreases to 4.0 (John & Marchal, 1995). The organic acid content of bananas at different ripening stages are shown in Table 2.6.

Table 2.6 The organic acid content of banana.
(meq/100g fresh wt)

Organic acid	**Stage of ripening**		
	Green	**Yellow/green**	**Fully Yellow**
Malic	1.36	5.37	6.20
Citric	0.68	1.70	2.17
Oxalic	2.33	1.32	1.37
Other acids	0.19	0.16	0.17
Total	4.43	8.74	10.90

Source: Caussiol (2001)

2.1.3.5 Nutrients

Table 2.7 shows the composition of unripe and ripe banana fruit, consists of high levels of minerals (especially K), oligosaccharides content, vitamins, oligosaccharides, and

phenolics (Caussiol, 2001; Youryon & Supapvanich, 2016). Therefore, bananas are considered one of high energy and nutrients fruit which has numerous health benefits (Huang, 2013).

Table 2.7 The typical composition of banana.
(g/100g edible portion of macronutrients and mg/100g of vitamins and minerals)

Composition	Unripe	Ripe
Water	71.9	75.2
Protein	1.9	1.7
Fat	0.1	0.1
Sugar	1.3	17.3
Starch	21.3	3.1
Dietary Fibre	3.2	2.8
Vitamin C	18.0	12.0
Carotene	0.2	0.1
Potassium	320.0	350.0
Calcium	5.0	5.0

Source: Caussiol (2001)

2.1.3.6 Carbohydrate

Carbohydrate content is variable between cultivars (Marriott et al., 1981). The accumulation of starch increased in the ripening period and then starch started to diminish when the fruit turned yellow (Caussiol, 2001). Starch is converted to sugars during banana ripening which gives sweetness to banana fruit (Goulao & Oliveira, 2008), pathways of conversion of starch into sugar are shown in Figure 2.3 (Seymour, 1993). The unripe banana fruit is mainly contained of starch which low sugar content while full ripe banana fruit is contained high sugar content (Table 2.8) (Marriott et al., 1981). Additionally, the starch sugar ratio is well correlated with peel color (Table 2.9) (Stover & Simmonds, 1987).

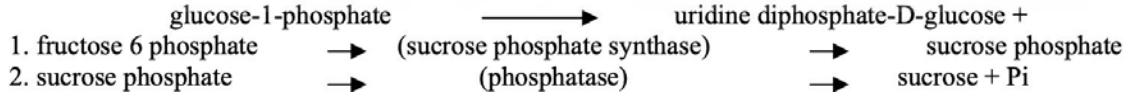

Figure 2.3 Pathways of conversion of starch into sugar.
Source: Caussiol (2001)

Table 2.8 The carbohydrate composition of banana.

Stage	Sugars (dry matter basis)	Sugars (fresh weight basis)
Unripe	2-8%	1%
Ripe	70-75%	18-20%

Source: Caussiol (2001)

Table 2.9 The relationship between peel color and carbohydrate of banana.

Stage	Peel color	Sugar (%)	Starch (%)
1	Green	0.5	20.0
Sprung	Green	1.0	19.5
2	Green-trace of yellow	2.5	18.0
3	More green than yellow	4.5	16.0
4	More yellow than green	7.5	13.0
5	Yellow-Green tip	13.5	7.0
6	Full Yellow	18.0	2.5
7	Yellow lightly flecked with brown	19.0	1.5
8	Yellow with increasing brown areas	19.0	1.0

Source: CSIRO (1972)

2.2 Microwave heating

2.2.1 Microwave heating background

Drying is a traditional method to preserve foods, it involves the reduction of moisture level in the food to prevent microbial spoilage. Microwave heating is one of alternative drying methods which is frequently used in the food industry, commonly used frequencies are 915 MHz and 2450 MHz (Huang, 2013). Traditional drying methods such as hot air drying are simple to use, however it has low energy efficiency and require longer drying time thus it is not economical. In addition, traditional drying methods which have long drying times at high temperatures during the falling rate periods may lead to undesirable colors in the dried end product and also occurs case-hardening of the food that affects the appearance but also the taste of the dried products (Mousa & Farid, 2002). Compared to traditional drying methods, microwave drying has more thermal efficiency which offers opportunities to shorten the drying time, thereby improving the quality and flavor of the end product (Huang, 2013).

2.2.2 Microwave heating principle

The principle of microwave heating differs from conventional heating. The microwave heating method dehydrates food by interactions between the electromagnetic energy and polar molecules within the material. Microwave energy as electromagnetic wave is transported in certain frequency bands, when the microwaves are applied to dielectric materials and impinge on them, part of the energy is transmitted, part is reflected and part is absorbed by the material which is dissipated form of heat (Huang, 2013).

Polar molecules such as water (H_2O) are oriented randomly but when an electric field is applied then they line up within it. In an alternating field, the microwave frequency being used to maintain their alignment of the polar molecules rotate which H-bonds between adjacent water molecules are disrupted during rotation thus generating heat (Figure 2.4). Additionally, the ions in solution (Na^+, Cl^- and Ca^{++}) in an electric field collide with other ions which the higher the number of ions in solution, the more frequent will be the collisions, and higher kinetic energy resulting in increased temperatures. Accordingly, water, carbon, and foods with high moisture content and compounds (e.g. salt and sugar) are good microwave absorbers (Huang, 2013).

Therefore, microwave heating is volumetric, rapid, and highly specific, which is no require contact between the energy source and the sample. It enhances the energy efficiency and has less negative impact on the quality of the dehydrated products (Maskan, 2000).

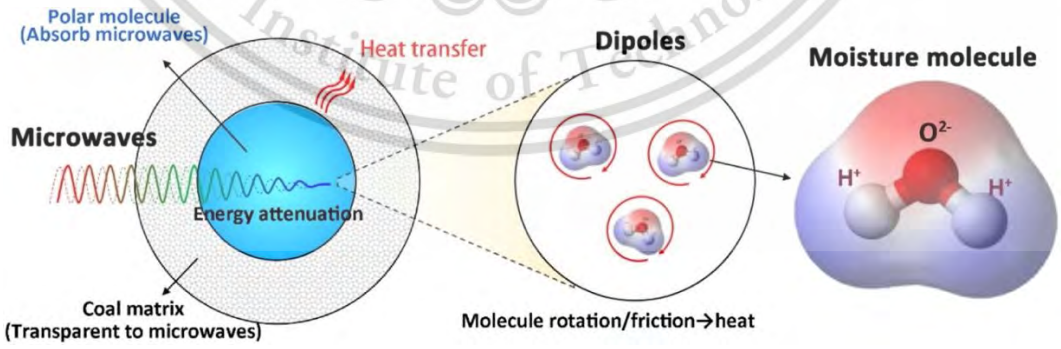

Figure 2.4 Mechanism of the microwave heating.
Source: Li et al. (2019) & Ju et al. (2021)

2.2.3 Parameters affecting microwave heating

Heating of materials by microwaves is affected by a number of properties of the equipment and the material being heated. The impact of each of these must be considered in the design of a processing system (Hui, 2009). These parameters are:

2.2.3.1 Frequency

In the field of industrial microwave heating, two frequencies as 915 and 2,450 MHz with the wavelengths of 0.33 and 0.122 m, respectively, are almost exclusively employed for all applications. Additionally, the frequency affects the depth of penetration into a material.

2.2.3.2 Microwave Power

Microwave power is the controlled variable in heating applications. It is a parameter with great effect on the value of both the centre and surface temperatures. The heating for a given mass is affected by the power output. In addition, varying the power output controls the speed of microwave heating. In a drying process, higher microwave power causes a rapid rise in product temperature (temperature runaway) and burnt of the dried product. Thus, the microwave power control strategies during the final drying phase are necessary in order to avoid temperature runaway and quality deterioration of the product.

2.2.3.3 Mass

Mass is one of the parameters affects the microwave drying and heating processes. There is a relationship between the mass and the amount of microwave power that applied to achieve the desired heating of the total mass. As for an individual particle, it will be explained under physical geometry and density.

2.2.3.4 Moisture content

The major parameter that effects the microwave power absorption of foods is water. Generally, the more of moisture content in food materials refer to the higher of the dielectric loss factor, resulting in better heating.

2.2.3.5 Density

The density of a product affects its dielectric constant. Commonly, the dielectric constant increases with density which is known to increase temperatures.

2.2.3.6 Temperature

The increasing or decreasing of dielectric loss with temperature is depend on the material. Thus, the initial temperature of food products which dehydrate by microwave heating should be known that the microwave power can be adjusted.

2.2.3.7 Physical Geometry

If the size of each individual piece is very large in comparison to the depth of penetration, the heating will not be uniform. Furthermore, heating is more uniform in regularly shaped bodies.

2.2.3.8 Conductivity

This describes the ability of a material to conduct electric currents by the displacement of electrons and ions, however dipolar rotation is the more frequently discussed means of generating heat in microwave systems where ionic conduction plays a major role in many cases, especially in foods containing salts.

2.2.3.9 Thermal conductivity

Thermal conductivity may have an important effect when heating large materials where the depth of penetration is not sufficient enough to heat uniformly up to the center or when the microwave heating time is long.

2.2.3.10 Specific heat

This is an often-neglected parameter in microwave heating, it can have an overriding influence on the heating, cause a material with a relatively low dielectric loss to heat well in a microwave field, resulting in a material heat faster.

2.2.4 Advantages and challenges

Microwave heating provides a rapid and efficient method for drying materials than the traditional drying process (Maskan, 2000). However, it has been seen that many factors affected microwave heating characteristics such as physical, thermal, and dielectric properties of the foods (Durance & Yaghmaee, 2011), which caused a non-uniform temperature distribution within the food thus eventually impact the quality of foods (Pitchai et al., 2014).

2.3 Temperature profile

Temperature is an important parameter in food processes and thermal properties determination. The temperature profiles of foods in relation to their properties and also thermal processing condition. Therefore, temperature profile is basically a thermal fingerprint for that food product in that particular heating process. In general, this thermal fingerprint provides information to analyze, improve, and ensure the uniformity of heat distribution in heat-treatment process (Sun et al., 1994), which will help control the food quality and ensure the issue of food safety (Ye et al., 2004). As the uniformity of temperature profile affects the quality of the food and also the issue of food safety (Kumar et al., 2014). Non-uniform temperature distribution may lead to create hot and cold spots within food material. A position that occurs hot spot risks in burning and case-hardening which caused quality loss of final food product (Ikediala et al.1999), while at a position that cold spot occurs can be a source of pathogens which can cause food-borne illness (Kumar et al., 2014). Thus, it is necessary to eliminate hot and cold spots or non-uniform temperature distribution during heat-treatment process of food materials.

2.4 Numerical method

2.4.1 Numerical method background

Numerical methods are techniques which approximate mathematical procedures for solving numerical problems. There are many types of the numerical methods used in modeling, such as Finite Element Method (FEM), Finite Volume Method (FVM), Finite Difference Method (FDM), etc. Numerical model is a representation of a physical behavior by using mathematical equations, based on relevant hypothesis and assumptions (Sirois & Grilli, 2015; Jones & Brischke, 2017). In addition, might be referred to the techniques which applied for numerically solving a set of equations that involves describing the physical problems, also referred as mathematical modeling (Larson, 2005).

2.4.2 Finite element methods

Finite element method (FEM) is a numerical discretization technique for solving a differential or integral equation and finding approximate solutions to Partial Differential Equations (PDEs) in physical modeling problems (Kampffmeyer, 2014) by divides the domain into elements (Wai et al., 2013). Each element is formulated with equations and the solution obtained by combined the

results (Felippa, 2004; Kampffmeyer, 2014; Liu et al., 2013; Logan, 2016). The FEM consists of assuming the piecewise continuous function and obtaining the parameters of the functions which for the solution and reduces the error, respectively (Dixit, 2007).

In FEM, there are many types of elements which are commonly classified into three groups; one-dimensional (1D) elements, two-dimensional (2D) elements, and three-dimensional (3D) elements (Figure 2.5). Actually, the model should be as close as possible to the actual structure thus it is an important for choosing the right element types to represent the model (Wai et al., 2013).

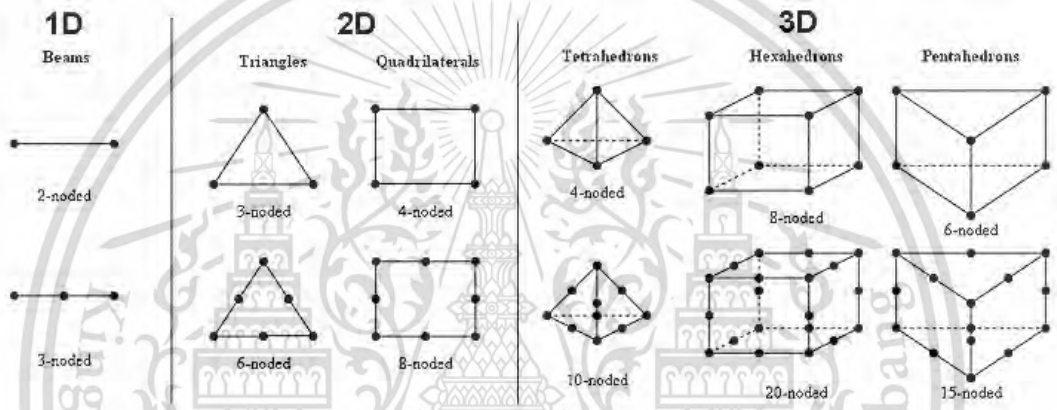

Figure 2.5 Different types of finite elements.
Source: Hadagali (2014)

2.4.3 Governing equations

Governing equations are a mathematical model which is a set of mathematical equations that describes a system behavior by represent the relevant properties relationship. There are many variables and parameters in mathematical equations. Variables are classified into two types which are independent and dependent variables, while parameters are as properties (e.g. temperatures). In addition, parameters which are affected by observer might be referred as adjustable, but the others set as constants. Mathematical model can be solved by determine the relations of dependent and independent variables, the solution depends on adjustable parameters values which yield specific required behavior by using mathematical models (Van Groesen & Molenaar, 2007).

2.4.4 Geometry

Computer-Aided Design (CAD) is the use of an application to create computer models defined by the geometry of the systems, computational geometry methods are used for handle irregular shapes and allowing to manipulate the shapes (Shabana, 2018). To solving problems in physics, CAD models are converted to a finite element (FE) mesh for analysis. In order to avoid the problems of numerical errors (e.g. spurious oscillations) which due to the geometry error from crude geometry approximations, an integrated approach is necessary to unifies CAD and FEA (Ernens, 2011).

2.4.5 Mesh

The finite element discretization contains nodes and elements, as shown in Figure 2.6 (Lei et al., 2020). A mesh generates by split the domain into a discrete number of elements which then join together with nodes, represents the shape of simple geometry. The solution of FEM is obtained by calculation the data which is interpolated across the whole domain, including both the external surface and the interior volume (Zhang, 2018).

In addition, the size of elements is very important, mesh that is chosen to be too dense will require more computational resources, while a mesh that is too sparse might cause the solution not to converge or will yield large approximation errors. Therefore, the FEM allows the size of these elements to vary across the modeling domain and it is therefore possible to reduce the element size around interfaces or complex structures to achieve high accuracy and resolution (Kampffmeyer, 2014). However, the error of the approximate solution not only depends on the size of the finite elements, but also on the position of the elements, which is why the mesh generation process is important (Kampffmeyer, 2014; Lo, 2002). The three main categories of mesh generation methods are structured, unstructured meshing, and hybrid meshing, as shown in Figure 2.7. All these methods have both advantages and disadvantages. The structured mesh, for example, benefits from the simplicity, while the unstructured mesh is more suitable for complex domains by offering better mesh adaptivity. Hybrid meshing combines the advantages of both methods by combining small structured meshes in a large unstructured mesh. It has, however, the disadvantage of being difficult to generate fully automatically (Bern & Plassmann, 2000; Kampffmeyer, 2014).

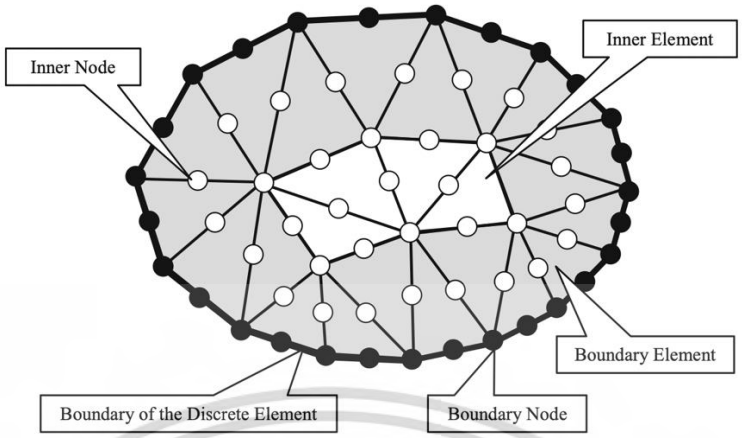

Figure 2.6 The domain with a group of finite elements and nodes.
Source: Lei et al. (2020)

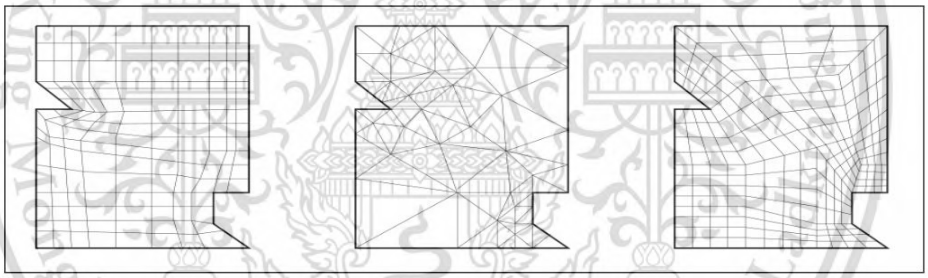

Figure 2.7 Meshing categories.
Source: Bern & Plassmann (2000) & Kampffmeyer (2014)

2.4.6 Boundary conditions

The boundary condition is a set of constraints, define the behavior of unknown functions on the spatial boundary of the domain. It is an important constraint for the solution of a boundary value problem. As a boundary value problem is a differential equation, which to be solved in a domain that is known a set of conditions of its boundary. Boundary value problems are extremely important with the model that enormous of phenomena and applications (e.g. from solid mechanics to heat transfer) (Cheng & Cheng, 2005).

2.5 COMSOL Multiphysics

COMSOL Multiphysics originates from MATLABs pde toolbox which could solve classical equations in 2D, it was used as modeling software. Over time, MATLABs was extended to support 3D scenarios and was called Femlab then Femlab was renamed to COMSOL Multiphysics in 2005 (Kampffmeyer, 2014).

2.6 Related research

There have been a number of studies involving microwave heating of foods which have essentially focused on using microwave energy for various food processes and looking at final food quality and other properties of the products due to microwave application. The process of microwave heating has also been studied with mathematically modeled by using analytical and numerical techniques. The following are the related research in this study:

Chen et al. (2016) studied on modeling heat and mass transport during microwave heating of frozen food rotating on a turntable. This study developed a comprehensive three-dimensional finite element model for describing microwave heating of a food product on a rotating turntable which including multiphysics of Maxwell's electromagnetic heating, energy conservation, Darcy's velocity, mass conservations of water and gas, and phase change of melting and evaporation of water. The spatial variation of the top surface temperatures of the mashed potato acquired by an infrared camera, the transient temperatures at six locations recorded by fiber optic sensors. With 83% reduction in computation time for the simplified approach, this method can be used to evaluate the microwave heating of food products and accelerate microwaveable food products development.

Gulati et al. (2016) developed a fundamentals-based coupled electromagnetics, multiphase transport and large deformation model to understand microwave drying of a hygroscopic porous material. Electric field distribution inside the oven cavity and porous material are obtained by solving Maxwell's equations for electromagnetics. Modes of fluid transport include capillarity, binary diffusion and gas pressure-driven flow. Large deformation, included by treating the solid as hyperelastic, is implemented in a novel way using the Arbitrary-Lagrangian–Eulerian framework for mesh movement. Deformation during microwave drying was found to critically alter material structure that significantly

affected microwave absorption, heat and moisture transport within the material. Sensitivity analysis revealed that moisture loss and volumetric shrinkage were unaffected with changes in intrinsic permeability and elastic modulus of the material while stress state within the material was highly sensitive to elastic modulus values.

Apinyavisit et al. (2018) investigated the heat and mass transfer longan shrinking from a regular spherical shape to an irregular shape during combined microwave with hot air drying (MHD), the heat and mass transfer coefficients equations for a spherical shape modified, and a moisture diffusivity equation as a function of temperature and moisture content also developed. The results indicated sensitivity analysis of the estimated parameters for the nonlinear equations indicated that global optimum values were determined.

Choudhary et al. (2018) developed a 2D finite element model to consider the simultaneous heat and mass transfer along with phase change effect during dehydration for predicting the temperature and moisture profiles of mushroom. The temperature and moisture content profiles, effect of convection and conduction heating, slowest heating zone (SHZ) were studied. The temperature profile of mushroom shows initial exponential increase followed by constant temperature during the drying process. Mushroom head portion showed higher moisture content when compared to stem as it also appears to be the slowest heating zone.

Esveld et al. (2018) measured the dielectric properties of starch based snack pellets in situ during microwave heating and expansion. The microwave setup consists of a single mode shorted waveguide, equipped with a six-port impedance analyzer which measures the absorbed power and complex reflection coefficient during heating. The dielectric properties of the pellet during heating and after expansion are obtained via an inverse mapping of the recorded reflection coefficient to dielectric properties, which are pre-computed via finite elements simulations. Experiments show that the dielectric properties of the starch pellets change significantly during heating, expansion and subsequent drying. The dielectric properties as function of temperature and moisture content were fitted with a polynomial model.

Huang et al. (2018) used a finite element method to study the influence of microwave settings to the heating effect of coal samples, a coupled mathematical model for electromagnetic, heat and mass

transfer in the process of microwave heating. This coupled model for microwave heating have considered heat and mass transfer, and is validated by comparison with experimental results. Then it is used to simulate the influence of frequency, power and moisture capacity on microwave heating. The simulation results show that microwave heating of coal is highly sensitive to excitation frequency.

Kumar et al. (2018) developed a comprehensive multiphase porous media model for apple drying. The model considered the transport of liquid water by capillary diffusion and gas pressure, and the transport of vapor by binary diffusion and gas pressure. A non-equilibrium formulation was used to calculate the evaporation rate, which enabled the separate illustration of vapor and liquid water transport. The equations were solved by finite element method (FEM) using physics-based modelling and a simulation platform (COMSOL Multiphysics). Spatial distribution of liquid water and vapor saturation curves showed the saturation levels were lower on and near the surface compared to the center of the food material. The convective and diffusive fluxes of liquid water and vapor were presented, and this data suggested that the fluxes were higher on and near the surface of the sample.

Naghavi et al. (2018) developed a three-dimensional model to simulate momentum, heat and mass transfer during deep-fat frying of uncoated or coated potato strips. The results revealed that different locations of potatoes did not have significant effect ($p > 0.05$) on the profiles of studied variables which can be used to provide valuable insight into the effect of food coating on transfer phenomena and may be very useful to optimize frying operation as well as to improve quality of coated potatoes during frying.

Zhang et al. (2018) studied on the effect of shape on the temperature field during microwave heating process, which was evaluated by microwave power absorption capability and temperature distribution uniformity in a single sample heated in a domestic microwave oven. The Maxwell equations were used to calculate the distribution of microwave electromagnetic field distribution in the microwave cavity and samples; then the electromagnetic energy was coupled as the heat source in the heat conduction process in samples.

Zhu et al. (2018) studied on a rotary radiation structure for microwave heating uniformity improvement. A simulation model has been built and computed based on the finite element method combined with programming. A quantitative validation of simulation results has been performed with

physical experiments. Heating uniformity and heating efficiency of the proposed method has been compared with two traditional methods, by which a potato slice is heated with a turntable and heated statically. The results show that the rotary radiation structure has an obvious superiority.

Albuquerque et al. (2019) studied on a 3D-CFD-heat-transfer-based model for the microbial inactivation of pasteurized food products. This study coupled a 3D-CFD and heat transfer finite elements model with the microbial inactivation. The CFD-heat transfer model was developed using thermophysical properties for both heating fluid (water) and the processed sample (ground beef). The inactivation kinetic parameters were found independent of the heating rate applied. A model could be beneficial in simulating microbial inactivation for food products, thus ensuring food safety by limiting, as far as possible, overtreatment.

Bianchi et al. (2019) developed a comprehensive multiphysics three-dimensional numerical model to investigate the couples electromagnetics, electrodynamics and heat and moisture transfer. As a result, arcing occurs at a lower power level because the equilibrium between ionization and attachment is achieved at lower electric field magnitude than in moist air. Higher temperature leads to greater chances of arcing as higher temperature increases ionization more than it increases attachment. Small load of food also increases the chances of arcing. Sample geometry, orientation, and placement inside the oven are also significant factors.

Gao et al. (2019) focused on the influence of various design parameters on microwave heating performance by coupling of the electromagnetic and the heat transfer equations by COMSOL Multiphysics software. The coupled model of microwave heating is numerically implemented using a finite element method and validated by comparison with previous experimental results. Results indicate that samples with different permittivities show different temperature rise. With some design parametric variations such as cavity shape, waveguide location, loading sample position and so on, the heating effects which are the energy utilization and temperature distribution exhibit sensitively. Furthermore, when the loading samples situate off the center of cavity, the heating effect is even better.

Hazervazifeh et al. (in press) investigated the effective design to reduce non-uniform heating in industrial microwave dryer. This study used finite element methods to monitor the electromagnetic field distribution, a simulation process. Three geometries were selected as the microwave cavity.

Analysis of variance for the indicator of heat non-uniformity index showed that cavity size has significant effect ($P < 0.05$) on the index. Experimental validation of simulated results proved that simulation can cover the pattern of temperature distribution with R^2 of 0.96.

Jain et al. (2019) developed a mathematical model for predicting electromagnetic power dissipation within a rectangular dielectric slab heated by equal intensity 915 MHz plane waves from top and bottom. A dimensionless parameter which is a combination of the loss factor, dielectric constant and food thickness was proposed. This unique number provided direct insight into the relationship between food dielectric properties, thickness, product temperature, and thermal lethality. A qualitative assessment of the combined effect of food properties on lethalities using this model will be helpful in process development for microwave assisted thermal sterilization (MATS) system.

Lentzou et al. (2019) studied on an optimization method for water diffusivity and peel resistance estimation with a moving boundary model for fruit isothermal drying and shrinkage. This study used a moving-boundary finite element model to describe fruits isothermal drying to estimate water diffusivity and peel resistance including shrinkage. The estimated resistance of the peel is found to be reduced by 62% as the drying temperature increases from 45 ℃ to 65 ℃ and by 55% as the drying temperature increases from 55 ℃ to 65 ℃. The proposed model predicts efficiently water content, shrinkage and water diffusivity.

Li et al. (2019) developed heat transfer and multiphase porous media model to investigate the drying kinetics of coal under microwave irradiation. Results show that the temperature rise of coal during microwave irradiation is characterized by fast-slow-fast, and water evaporation is the key factor in thermal distribution. The water in the hot spot decreases, while the vapor increases and migrates towards the cold spot. The saturation time of the water always lags behind that of the vapor. In addition, the higher the microwave power, the quicker the fluid reaches the ultimate value. The non-uniform microwave heating enhances the thermal gradient and gas pressure gradient in coal, leading to irreversible damage.

Onwude et al. (2019) studied on an intermittent infrared and convective drying of sweet potato (*Ipomoea batatas* L.). This study developed a physics based mathematical model to understand the mechanism of drying sweet potato using intermittent infrared and convective drying (IIRCD),

COMSOL Multiphysics finite element software was employed for the model simulation. The model was based on shrinkage dependent diffusivity and evaporation phenomenon. As a result, drying of sweet potato using IIRCD was found to be more efficient in terms of final product quality compared to convective hot-air drying method.

Purlis (2019) presented a theoretical and numerical analysis to derive a multiphase model of heat and mass transfer for low intensity/temperature convective drying of hygroscopic porous materials, with focus on food products, which is important to understand the underlying physics of the process.

Upadhyay and Rai (2019) studied on a new iterative least square Chebyshev wavelet Galerkin finite element method applied to dual phase lag model on microwave drying of foods. This study developed a dual-phase-lag (DPL) model of heat and mass transfer in presence of a source term for microwave drying foods of different geometrical configuration like slab, cylinder or sphere under the most generalized boundary conditions.

Hosseini et al. (2020) developed a model-based controller for moisture distribution in an industrial microwave drying process. The moisture and temperature in the process are described by a pair of partial differential equations (PDEs) and have both temporal and spatial variations. This study used a semi-discrete finite element approximation, the coupled system of PDEs is transformed into a system of ordinary differential equations (ODEs). The results show that the proposed controller achieves a very good performance in tracking the desired moisture level.

Huang et al. (2020) established three-dimensional multiphysics-based models with a commercial finite element (FE) simulation package (COMSOL Multiphysics) to analyze the radio frequency (RF) disinfestation process of dried apricots by defining six sub-domains: the flesh, a thin air layer, pit, air layer, kernel, and Indian meal moth larva located on the apricot surface. Model prediction results demonstrated that compared with other physical locations (insect in perfect/partial contact with the flesh), the focusing effect of electric fields caused relatively fast heating rate (10.2 °C min^{-1}) and high average temperature (68 °C) when the insects were located on the fruit surface (in point contact with flesh). Thus, the focusing effect of electric fields within insect body plays an important role in efficacy of RF disinfestation treatment for dried fruit.

Roohi and Hashemi (2020) used the coupled 3D and transient form of heat and Maxwell's equations to determine the temperature distribution within a carrot slice in the microwave cavity during pasteurization as a clean and energy saving process. Based on the obtained results the energy demand of the microwave thermal treatment was 52.3% lower than conventional steam surface pasteurization and also it can be used as a clean process in pasteurization of carrots instead of chemical pasteurization.

Shen et al. (2020) studied on modelling of moving drying process and analysis of drying characteristics for germinated brown rice (GBR) under continuous microwave drying, the heat and mass transfer were investigated numerically and experimentally. As a result, The movement of materials can effectively reduce excessive absorption of microwave energy by the grain layer, and achieve uniform distribution of temperature and moisture content and high drying uniformity assisted by the synergistic effects of microwave heating, moisture evaporation and ventilation convection. The developed model and simulation strategy may provide guidance for understanding and analysis of continuous microwave drying process of granular materials such as GBR.

Zhou et al. (2020) studied on a novel algorithm approach for rapid simulated microwave heating of food moving on a conveyor belt. In this work, a novel algorithm method is proposed to for rapid simulated microwave heating of food moving on a conveyor belt. The calculation results show that compared with the conventional method, the calculation efficiency of the proposed method is improved by 572%. Moreover, the proposed method does not require mesh reconstruction, and the proposed method is also applicable to radio frequency moving heating. The feasibility and accuracy of the method were verified by experimentally measuring the temperature change.

Acevedo et al. (2021) studied on the exergy transfer principles of microwavable materials under electromagnetic effects. This study presented heat transfer and exergy transfer which focused on those materials with high interactions with microwaves (susceptors). The heat transfer studies demonstrated the way microwaves are transformed into heat, and the exergy analysis shows the quality of those transformations. Exergy transfer analysis of microwave heating systems sheds light on the efficiency of the energy transformation taking place during microwave processing. Consequently, by combining studies of microwavable materials with exergy transfer analysis, conclusions for new microwave designs can be reached, improving this promising technology's final performance. In this sense, this work provides an easy method to determine different materials' behavior under microwave effects.

Renshaw et al. (2021) studied on mathematical modelling of dielectric properties of food with respect to moisture content using adapted water activity equations. This study addresses this issue so that moisture dependant dielectric properties can be directly input into drying models, where the microwave or radio frequency source is always limited to a single frequency. As a result, the adapted water activity equations proved to be very effective at describing dielectric behavior.

Selimefendigil et al. (2021) used three-dimensional numerical study of convective drying process was investigated for two porous moist blocks in a channel under turbulent flow conditions by considering different parameters which are effective on heat and moisture transfer phenomena. Drying objects were rectangular shaped porous objects and effects of size and distance between the objects, velocity and temperature of inlet drying air were investigated with varying values. Obtained results showed that all of the changing parameters had significant effects on flow properties, heat and mass transfer phenomena in 3D.

Ye et al. (2021) used a hybrid Arbitrary Lagrange Eulerian (ALE)/implicit function method for simulating microwave heating with rotating objects of arbitrary shape. A 2D model and a 3D model with rotating objects in irregular shapes are used to illustrate the proposed method. the results show that, for dealing with the cases with moving objects in complex shapes, this method is much more accurate and efficient than the ALE-remeshing method.

Yi et al. (2021) studied on a simulation method of coupled model for a microwave heating process with multiple moving elements. In this study, a stepping algorithm based on implicit function and level set method is proposed to simulate the microwave heating process of multi-component with unequal moving speed. The results show that the proposed model can effectively improve the heating uniformity and heating efficiency.

CHAPTER 3

MATERIALS AND MEDTHODS

3.1 Raw materials

Bananas [*Musa sapientum* Linn. (ABB group) 'Kluai Namwa'] that had similar characteristics with no evidence of mechanical damage were purchased from a local market. The bananas were classified according to a peel color index, CSIRO (CSIRO, 1972).

3.2 Instruments and equipment

3.2.1 800 W Microwave oven (SHARP R-299, Sharp Thai Co., Ltd., Thailand)

3.2.2 Thermal imaging camera (FLIR E40, FLIR Systems, Inc., United States)

3.2.3 Computer workstation based on the Intel Xeon E7 and 32 GB of RAM

3.3 Research methodology

3.3.1 FE modeling of temperature distribution of banana during microwave heating process to study the effects of ripening stages and shapes

3.3.1.1 Experiment procedures

3.3.1.1.1 Study on the effect of ripening stages

Unripe banana (stage 1) and ripe banana (stage 6) were selected as samples for this study (Figure 3.1). The banana samples from each ripening stage were peeled and sliced into a transversal shape, with dimensions as shown in Table 3.1.

3.3.1.1.2 Study on the effect of shapes

Ripe banana (stage 6) was selected as samples for this study. The banana samples were peeled and sliced into two different shapes (transversal and longitudinal), with dimensions as shown in Table 3.1.

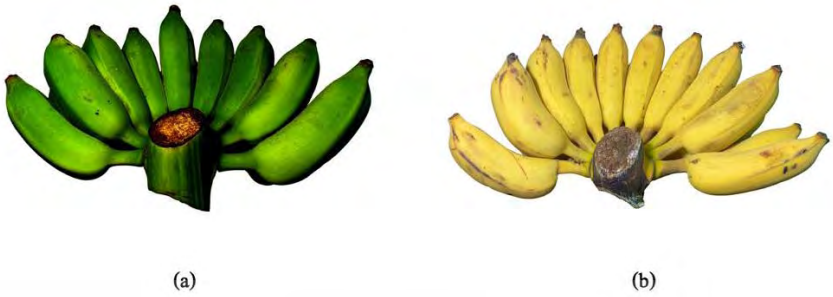

(a) (b)

Figure 3.1 Banana samples; (a) unripe banana; (b) ripe banana.

Table 3.1 Banana dimensions.

Parameter	**Value**	**Unit**
Transversal shape ($D \times h$)	30 × 5	mm
Longitudinal shape ($w \times d \times h$)	30 × 100 × 5	mm

3.3.1.1.3 Microwave heating condition

A sample was placed on the center of the turntable plate inside the microwave oven cavity. Heating was performed in a microwave oven using the maximum level at 800 W for 60 s. The microwave experiment setup scheme is shown in Figure 3.2. Each experiment was performed in triplicate in order to obtain average temperature data.

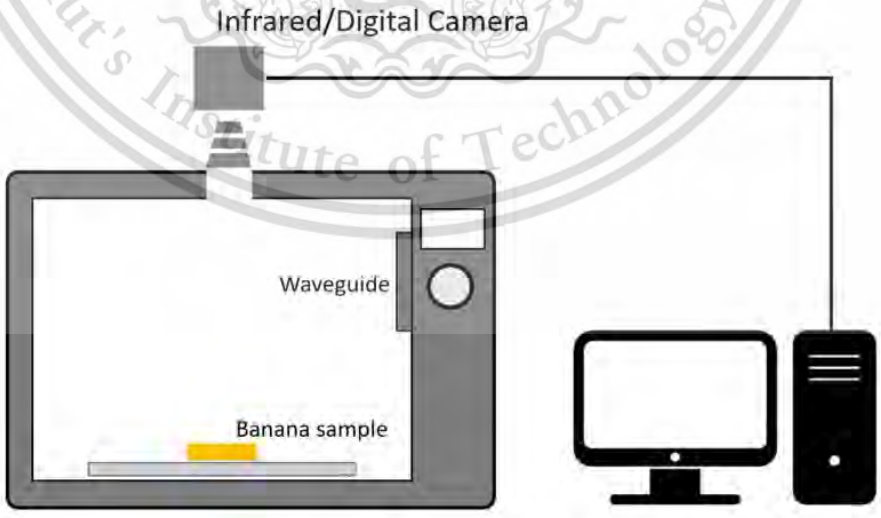

Figure 3.2 Schematic diagram of microwave heating experimental.

3.3.1.1.4 Measurement of temperature distribution during microwave heating

The dehydration temperatures of a banana sample were monitored and recorded using a thermal imaging camera at an interval of 10 s. Temperature monitor points were defined at measurement positions, the specific positions of each shape which observed in this study are shown in Figure 3.3.

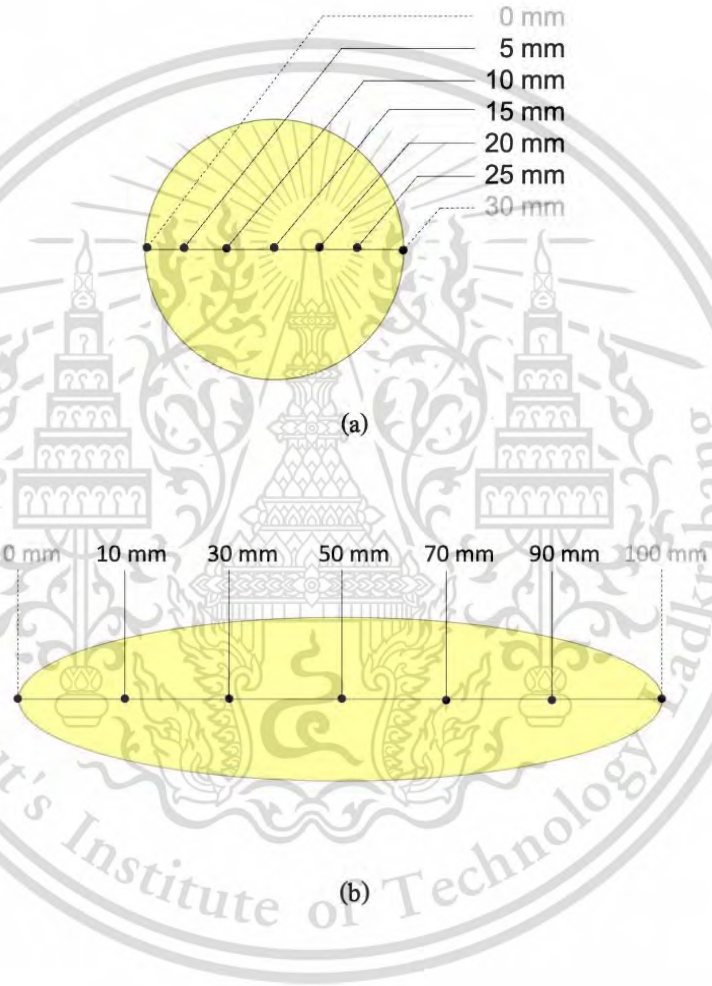

Figure 3.3 The specific temperature measurement positions;

(a) transversal; and (b) longitudinal.

3.3.1.2 FE modeling

3.3.1.2.1 Assumptions

In order to avoid numerical errors, some assumptions were made to simplify the problem. These assumptions were as follows:

- The input parameter values of banana for the model that used in this study were collected from the literature which varieties of bananas are assumed negligible.
- The initial temperature of banana was considered as homogeneous and isotropic.
- The temperature at which a real gas obeys the ideal gas laws.
- Heat capacity, dielectric constant, coefficient of thermal expansion of banana sample remains constant during simulation.
- The mass and momentum transfer of moisture were not considered.
- Chemical reaction is neglected.
- The shrinkage and puffing of banana are assumed negligible.
- The air temperature (inside cavity) around a banana sample is not influence by microwave heating and hence remains constant.
- The turntable is assumed to be in isothermal.
- The rotation motion of the turntable in the microwave cavity is not accounted.
- The equation of energy balance of the air (inside cavity) and turntable is not solved.
- Electromagnetic field around a banana sample presents TE_{10} mode.
- Simulation was performed by considering a single 2.45 GHz magnetron frequency.

3.3.1.2.2 Governing equations

For solving the heat distribution in the material, two kinds of mathematical models, namely, the electromagnetic field analysis model (EM model) and the heat transfer analysis

model (HT model), were associated together. The internal heat generation of the material, which was used in the HT model to predict the temperature distribution, was obtained by solving the EM model (Liu et al., 2013).

The electromagnetic field distribution inside the microwave oven for heating food material is governed by Maxwell's equations (Rakesh et al., 2012):

$$\nabla \times E = -j\omega\mu H \quad \text{(Eq. 1)}$$

$$\nabla \times H = j\omega\varepsilon_0\varepsilon E \quad \text{(Eq. 2)}$$

$$\nabla \cdot E = 0 \quad \text{(Eq. 3)}$$

$$\nabla \cdot H = 0 \quad \text{(Eq. 4)}$$

where E is the electric field intensity (V/m); H is the magnetic field intensity (A/m); ω is the angular frequency (rad/s); ε_0 is the permittivity of free space (8.854 x 10^{-12} F/m); j is the complex number operator, and ε is the complex relative permittivity, which is defined as

$$\varepsilon = \varepsilon' - j\varepsilon'' \quad \text{(Eq. 5)}$$

where ε' is the dielectric constant, and ε'' is the dielectric loss factor.

Based on Maxwell's equations, the following equation is solved to determine the electric field distribution inside a microwave oven cavity (COMSOL, 2015; Pitchai et al., 2014)

$$\nabla \times (\mu_r^{-1}\nabla \times E) - k_0^2\left(\varepsilon_r - \frac{j\sigma}{\omega\varepsilon_0}\right)E = 0 \quad \text{(Eq. 6)}$$

where μ_r is the relative permeability of the food material; ε_r is the relative permittivity; k_0 is the wave number, and σ is the electrical conductivity (S/m).

The equation below shows the complex of factors for the conversion of electromagnetic energy into thermal energy (Pitchai et al., 2014)

$$Q_m = \pi f \varepsilon_0 \varepsilon'' E^2 \quad \text{(Eq. 7)}$$

where Q_m is the heat generation due to microwaves (W/m^3); f is the frequency (Hz), and ε'' is the dielectric loss factor.

The thermal and heat transfer conditions were applied by Fourier's energy balance equation as follows (Khan et al., 2020)

$$\rho C_p \frac{\partial T}{\partial t} = \nabla \cdot \left(k_{eff} \nabla T\right) + Q_m \quad \text{(Eq. 8)}$$

where ρ is the density of the sample $(\mathrm{kg/m^3})$; C_p is the specific heat of material $(\mathrm{J/kg\ K})$; T is the temperature of the sample (K); k_{eff} is the effective thermal conductivity $(\mathrm{W/m\ K})$, and Q_m is the heat generation due to microwaves $(\mathrm{W/m^3})$.

3.3.1.2.3 Geometry

- Microwave oven

The geometric model of the microwave system used in this study was developed based on the real structure and size of the domestic 800 W microwave oven that was used in the experimental procedures. It was composed of an oven cavity, waveguide, and turntable (glass plate), as shown in Figure 3.4, and the dimensions are given in Table 3.2. The excitation for the microwave oven is through a rectangular waveguide. At an excitation frequency of 2.45 GHz, the TE_{10} mode is the only propagation mode (COMSOL, 2015).

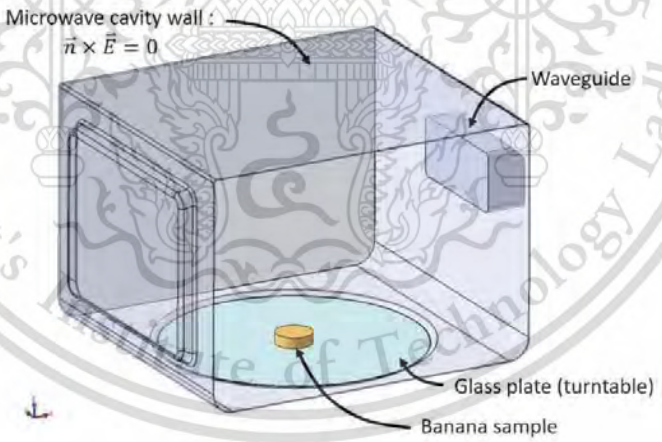

Figure 3.4 The geometrical model.

Table 3.2 The dimensions of a microwave oven.

Parameter	Value	Unit	Source
Oven cavity dimensions $(w \times d \times h)$	319 × 336 × 204	mm	(SHARP, 2013)
Waveguide dimensions $(w \times d \times h)$	50 × 78 × 18	mm	(SHARP, 2013)
Turntable diameter	272	mm	(SHARP, 2013)

- Banana

The geometry of the banana samples was generated into two different geometries: transversal and longitudinal, as shown in Figure 3.5, and the dimensions of banana samples are given in Table 3.1.

Figure 3.5 The geometries of banana slice used for simulation;
(a) transversal; and (b) longitudinal.

3.3.1.2.4 Mesh

To achieve a good prediction accuracy and reduced computational time, the geometric models require an appropriate mesh size for the domains. Tetrahedral elements were assigned to the domains, including the oven cavity, waveguide, turntable, banana sample and air in the oven cavity. The main research objective of this paper is to investigate the heat distribution of the banana; therefore, extremely fine mesh refinement levels were enforced for the banana sample, while fine mesh refinement levels were selected for the other domains. The computational domain for the heat distribution was used for the banana sample only. Figure 3.6 shows the meshing scheme of the microwave oven and the banana sample.

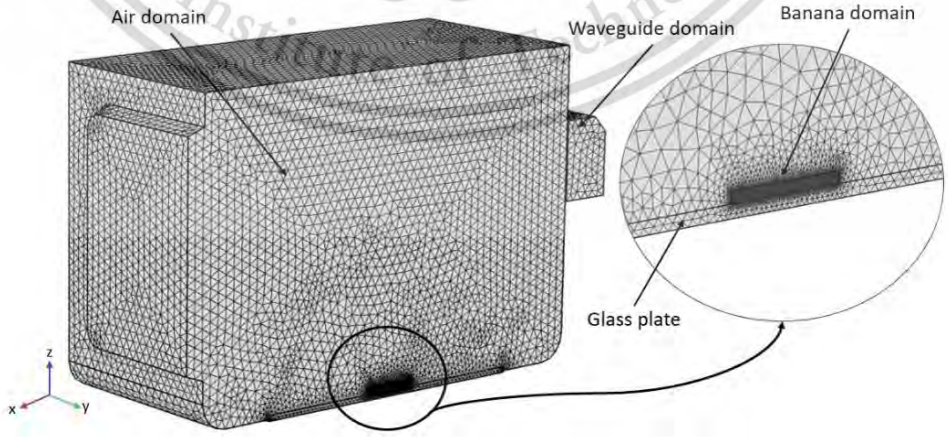

Figure 3.6 Meshing scheme of the materials.

3.3.1.2.5 Boundary conditions

In a microwave oven cavity, the walls of the cavity are considered to be perfect electrical conductors, where the following boundary condition applies

$$E_{tangential} = 0 \quad \text{(Eq. 9)}$$

3.3.1.2.6 Input parameters and initial conditions

The input parameters and initial conditions in this study were summarized in Table 3.3.

Table 3.3 Input parameters and initial conditions used in the simulations.

Parameter	Value	Unit	Source
Heating time	60	s	This study
Microwave frequency	2450	MHz	(SHARP, 2013)
Density			
- Unripe banana	1320	kg/m^3	(Udomdetwatthana, 1993)
- Ripe banana	870	kg/m^3	(Udomdetwatthana, 1993)
Specific heat			
- Unripe banana	2430	J/kg K	(Udomdetwatthana, 1993)
- Ripe banana	3430	J/kg K	(Udomdetwatthana, 1993)
Thermal conductivity			
- Unripe banana	0.41	W/m K	(Udomdetwatthana, 1993)
- Ripe banana	0.97	W/m K	(Udomdetwatthana, 1993)

3.3.1.2.7 Numerical solution

In this study, a computer workstation with COMSOL Multiphysics software was selected for solving the mathematical models by use of the FEM. FEs are analyzed in the simulations by the mesh in the domains, utilizing numerical solvers (Figure 3.7) (Malafronte et al., 2012).

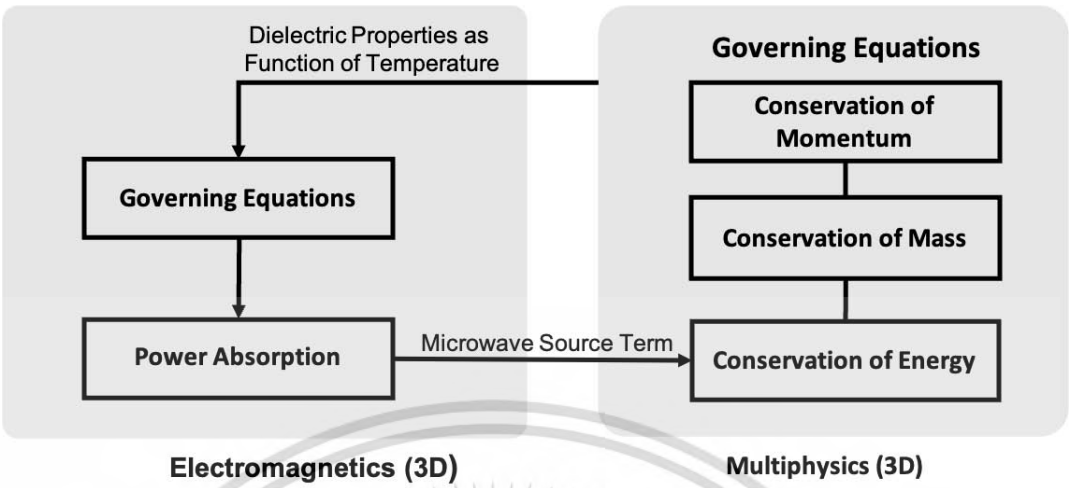

Figure 3.7 Flow chart of the computational model.

3.3.1.2.8 Model validation

To validate the simulation results, the simulated temperature profiles were compared with the data collected from the experiment. The accuracy of the simulation results was assessed by determining the coefficient of determination (R-squared; R^2). Note that the maximum value of R-squared is 1.0, which indicates a perfect prediction. In general, a value above 0.75 normally indicates a useable result (Liew & Lau, 2012).

3.3.2 Finite element modeling of temperature distribution of banana during microwave heating process to study of dehydration phenomenon of banana slices during microwave heating

3.3.2.1 Experiment procedures

The sample preparation and also microwave heating condition in this study were same as the procedures which study on the effect of ripening stages, as described in 3.3.1.1.1 and 3.3.1.1.3. In addition, moisture loss was determined through weighing the sample during the experimentation; the sample was taken out from the microwave oven cavity, weighed on a digital balance, with weights recorded at every 10 s, and placed back into the cavity immediately after weighing. The dehydration procedure was repeated, and the dehydration experiment was stopped at 60 s of heating time.

3.3.2.2 FE modeling

3.3.2.2.1 Assumptions

To avoid numerical errors, some assumptions were made to simplify the problem. These assumptions were as follows:

- The input parameter values of banana for the model that used in this study were collected from the literature which varieties of bananas are assumed negligible.
- The initial temperature of banana was considered as homogeneous and isotropic.
- Heat capacity, dielectric constant, coefficient of thermal expansion of banana sample remains constant during simulation.
- The banana sample is considered as a porous medium, and the pores are filled with three transportable phases: liquid water, air, and water vapor.
- Local thermodynamic equilibrium exists. Thus, the solid, liquid, and gas phases are at the same average temperature at any moment in the control volume.
- Solid, liquid, and gas phases are continuous.
- The binary gas mixture of air and vapor obeys the ideal gas law.
- The non-equilibrium condition prevails during evaporation.
- Evaporation takes place throughout the entire domain.
- Chemical reaction is neglected.
- The shrinkage and puffing of banana are assumed negligible.
- The air temperature (inside cavity) around a banana sample is not influence by microwave heating and hence remains constant.
- The turntable is assumed to be in isothermal.
- The rotation motion of the turntable in the microwave cavity is not accounted.
- The equation of energy balance of the air (inside cavity) and turntable is not solved.

- Electromagnetic field around a banana sample presents TE_{10} mode.
- Simulation was performed by considering a single 2.45 GHz magnetron frequency.

3.3.2.2.2 Governing equations

3.3.2.2.2.1 Electromagnetic field and heat generation

The heat distribution in the material in this study was obtained by solving (Eq. 1) – (Eq. 7) which described in 3.3.1.2.2.

3.3.2.2.2.2 Multiphase porous media transport model

In this study, a banana sample was considered as a porous medium, and the pores were filled with three transportable phases: liquid water, air, and water vapor (Kaviany, 2012; Kumar et al., 2016). The heat and mass transfer phenomena in the sample and also the phase changes in the porous media during microwave heating are shown in Figure 3.8. The multiphase heat and mass transport model with an additional heat generation term, calculated from the electromagnetic field distribution of the porous media, can be solved by the governing equations: mass and momentum balance equations, mass balance equations for the gas phase, energy balance equations, and evaporation rate. In this study, these governing equations are explained in detail as in Ni et al. (1999) and Kumar et al. (2016).

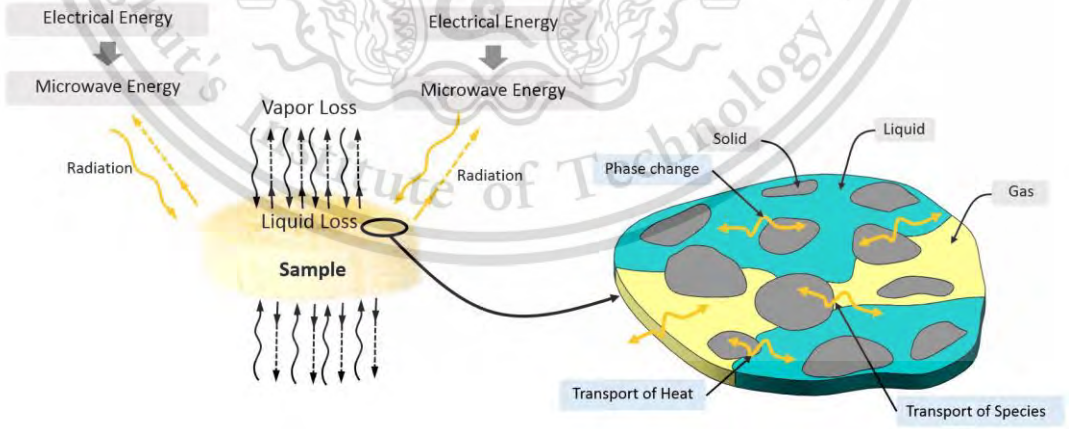

Figure 3.8 Heat and mass transfer of a sample with representative elementary volume (REV) showing transport, reaction, and phase change in porous media.

- Mass and momentum balance equations

The representative elementary volume is the sum of the volume of three phases: gas, liquid (water), and solid; thus,

$$\Delta V = \Delta V_g + \Delta V_w + \Delta V_s \quad \text{(Eq. 10)}$$

where ΔV is the representative elementary volume (m^3); ΔV_g is the volume of gas (m^3); ΔV_w is the volume of water (m^3), and ΔV_s is the volume of solid (m^3).

Equivalent porosity is defined as

$$\varphi = \frac{\Delta V_g + \Delta V_w}{\Delta V} \quad \text{(Eq. 11)}$$

where φ is the equivalent porosity.

Equivalent saturations of liquid and gas are defined as

$$S_w = \frac{\Delta V_w}{\Delta V_w + \Delta V_s} = \frac{\Delta V_w}{\varphi \Delta V} \quad \text{(Eq. 12)}$$

and

$$S_g = \frac{\Delta V_g}{\Delta V_w + \Delta V_g} = \frac{\Delta V_g}{\varphi \Delta V} = 1 - S_w \quad \text{(Eq. 13)}$$

where S_w is the equivalent saturation of water, and S_g is the equivalent saturation of gas.

The mass densities of vapor, air, and their mixture are given by

$$\rho_v = \frac{\Delta m_v}{\Delta V_g} = \frac{p_v M_v}{RT} \quad \text{(Eq. 14)}$$

$$\rho_a = \frac{\Delta m_a}{\Delta V_g} = \frac{p_a M_a}{RT} \quad \text{(Eq. 15)}$$

$$\rho_g = \frac{\Delta m_v + \Delta m_a}{\Delta V_g} = \frac{P M_g}{RT} = \rho_v + \rho_a \quad \text{(Eq. 16)}$$

where ρ_v is the mass density of vapor (kg/m^3); ρ_a is the mass density of air (kg/m^3); ρ_g is the mass density of gas (kg/m^3); p_v is the partial pressure of vapor (Pa); p_a is the partial pressure of air (Pa); P is the total pressure (Pa); M_v is the molar mass of vapor (kg/mol); M_a is the molar mass of air (kg/mol); M_g is the molar mass of gas (kg/mol); Δm_v is the mass of vapor in a representative elementary volume (kg); Δm_a is the mass of air in a representative elementary volume (kg); R is the universal gas constant (J/mol K), and T is the temperature of the material (K).

For the gas mixture of air and vapor, the total pressure is given by

$$P = p_v + p_a \quad \text{(Eq. 17)}$$

The mass concentrations of vapor, air, and liquid water are given by

$$c_v = \frac{\Delta m_v}{\Delta V} = \frac{p_v M_v \varphi S_g}{RT} \quad \text{(Eq. 18)}$$

$$c_a = \frac{\Delta m_a}{\Delta V} = \frac{p_a M_a \varphi S_g}{RT} \quad \text{(Eq. 19)}$$

$$c_w = \frac{\Delta m_w}{\Delta V} = \frac{\rho_w \Delta V_w}{\Delta V} = \rho_w \varphi S_w \quad \text{(Eq. 20)}$$

where c_v is the mass concentration of vapor ($\mathrm{kg/m^3}$); c_a is the mass concentration of air ($\mathrm{kg/m^3}$); c_w is the mass concentration of liquid water ($\mathrm{kg/m^3}$); Δm_w is the mass of liquid water in a representative elementary volume (kg), and ρ_w is the density of water ($\mathrm{kg/m^3}$).

The mass conservation equation for liquid water considers gas pressure driven flow, capillary diffusion, and evaporation of liquid water to vapor. The equations for the mass concentration of liquid water can be written as

$$\frac{\partial}{\partial t}(\varphi S_w \rho_w) + \nabla \cdot \left(-\rho_w \frac{k_w k_{r,w}}{\mu_w} \nabla P - D_c \nabla c_w\right) = -R_{evap} \quad \text{(Eq. 21)}$$

where k_w is the intrinsic permeability of water ($\mathrm{m^2}$); $k_{r,w}$ is the relative permeability of water; μ_w is the viscosity of water (Pa s); D_c is the capillary diffusivity ($\mathrm{m^2/s}$), and R_{evap} is the evaporation rate of liquid water to water vapor ($\mathrm{kg/m^3 s}$).

The mass balance equation for the vapor component of the gas phase includes bulk flow, binary diffusion, and phase change, and is given by

$$\frac{\partial}{\partial t}(\varphi S_g \rho_g \omega_v) + \nabla \cdot \left(-\rho_g \omega_v \frac{k_g k_{r,g}}{\mu_g} \nabla P - \varphi S_g \rho_g D_{eff,g} \nabla \omega_v\right) = R_{evap} \quad \text{(Eq. 22)}$$

where ω_v is the mass fraction of vapor; k_g is the intrinsic permeability of gas ($\mathrm{m^2}$); $k_{r,g}$ is the relative permeability of gas; μ_g is the viscosity of gas (Pa s), and $D_{eff,g}$ is the binary diffusivity of vapor and air ($\mathrm{m^2/s}$).

The mass fraction of air can be calculated from the expression

$$\omega_a = 1 - \omega_v \quad \text{(Eq. 23)}$$

where ω_a is the mass fraction of air.

- Mass balance equations for the gas phase

The overall mass balance for the gas phase is defined as

$$\frac{\partial}{\partial t}(\varphi S_g \rho_g) + \nabla \cdot \left(-\rho_g \frac{k_g k_{r,g}}{\mu_g} \nabla P\right) = R_{evap} \quad \text{(Eq. 24)}$$

- Energy balance equation

The energy balance equation is described by the following equation:

$$\rho_{eff} c_{peff} \frac{\partial T}{\partial t} + \nabla \cdot \left(\vec{n}_g h_g + \vec{n}_w h_w\right) = \nabla \cdot \left(k_{eff} \nabla T\right) - h_{fg} R_{evap} + Q_m \quad \text{(Eq. 25)}$$

where $\vec{n}_w$ is the water flux (kg/m^2 s); $\vec{n}_g$ is the gas flux (kg/m^2 s); T is the temperature of each phase (K); h_g is the enthalpy of gas (J); h_w is the enthalpy of water (J); h_{fg} is the latent heat of evaporation (J/kg); ρ_{eff} is the effective density (kg/m^3); c_{peff} is the effective specific heat (J/kg K), and k_{eff} is the effective thermal conductivity (W/m K).

The flux of water and gas can be calculated from the expression:

$$\vec{n}_w = -\rho_w \frac{k_w k_{r,w}}{\mu_w} \nabla P - D_c \nabla c_w \quad \text{(Eq. 26)}$$

and

$$\vec{n}_g = -\rho_g \omega_v \frac{k_g k_{r,g}}{\mu_g} \nabla P - \varphi S_g \rho_g D_{eff,g} \nabla \omega_v \quad \text{(Eq. 27)}$$

The effective properties taking mass and volume changes are described by following equations:

$$\rho_{eff} = \varphi\left(S_g \rho_g + S_w \rho_w\right) + (1 - \varphi)\rho_s \quad \text{(Eq. 28)}$$

$$c_{peff} = m_g(\omega_g c_{pg} + \omega_a c_{pa}) + m_w c_{pw} + m_s c_{ps} \quad \text{(Eq. 29)}$$

$$k_{eff} = \varphi(S_g k_{th,g} + S_w k_{th,w}) + (1 - \varphi) k_{th,s} \quad \text{(Eq. 30)}$$

where ρ_s is the solid density $(\mathrm{kg/m^3})$; c_{pg}, c_{pw}, and c_{ps} are the specific heat capacities of gas, water, and solid $(\mathrm{J/kg\ K})$, respectively; $k_{th,g}$, $k_{th,w}$, and $k_{th,s}$ are the thermal conductivities of gas, water, and solid $(\mathrm{W/m\ K})$, respectively, and m_g, m_w, and m_s are the mass fractions of gas, water, and solid (kg), respectively.

- Evaporation rate

The evaporation rate can be calculated from the expression:

$$R_{evap} = K_{evap} \frac{M_v}{RT}(p_{v,eq} - p_v) \quad \text{(Eq. 31)}$$

where K_{evap} is the evaporation constant $(1/\mathrm{s})$, and $p_{v,eq}$ is the equilibrium vapor pressure (Pa).

3.3.2.2.3 Geometry

The geometric model of the microwave system used in this study was same as described in 3.3.1.2.3. However, the geometry of the banana with transversal shape was only selected as a sample in this study, detail of geometry also as described in 3.3.1.2.3.

3.3.2.2.4 Mesh

Mesh qualities of microwave oven and the banana sample in this study were same as described in 3.3.1.2.4.

3.3.2.2.5 Boundary conditions

A microwave oven cavity, the walls of the cavity are considered to be perfect electrical conductors, where boundary condition applies by (Eq. 9).

The boundary conditions for heat and mass transfer at the transport boundaries of the food sample for this study are similar in their detail to those of Rakesh et al. (2012) and Kumar et al. (2016).

The heat and mass transfer that take place at the transport boundaries are described by the following equations

$$\vec{n}_{w,s} = h_{mv}\varphi S_w \frac{(p_v - p_{v\,air})}{RT} \quad \text{(Eq. 32)}$$

and

$$\vec{n}_{v,s} = h_{mv}\varphi S_g \frac{(p_v - p_{v\,air})}{RT} \quad \text{(Eq. 33)}$$

where $\vec{n}_{w,s}$ is the total water flux at the surface (kg/m^2 s); $\vec{n}_{v,s}$ is the total vapor flux at the surface (kg/m^2 s); h_{mv} is the mass transfer coefficient (m/s), and $p_{v,air}$ is the vapor pressure of ambient air (Pa).

The pressure was set to ambient at all surfaces of the sample. The boundary condition can be expressed as

$$P = P_{amb} \quad \text{(Eq. 34)}$$

where P_{amb} is the ambient pressure (Pa).

The loss of heat due to the evaporation of water and the removal of liquid water and vapor is also included in the boundary condition for heat transfer, and it can be expressed as

$$q_{surf} = h_T(T - T_{air}) - h_{mv}\varphi S_w \frac{(p_v - p_{v,air})}{RT} h_{fg} - h_{mv}\varphi S_g \frac{(p_v - p_{v,air})}{RT} C_v T \quad \text{(Eq. 35)}$$

where h_T is the heat transfer coefficient (W/m^2K); T_{air} is the drying air temperature (K), and C_v is the specific heat of vapor at a constant volume ($J/kg\,K$).

3.3.2.2.6 Input parameters and initial conditions

The input parameters and initial conditions in this study were same as listed in Table 3.3 and also added more input parameters from Table 3.4.

3.3.2.2.7 Numerical solution

The solution in this study was same as described in 3.3.1.2.7, additionally, the coupling of physics and the solution process is shown in Figure 3.9.

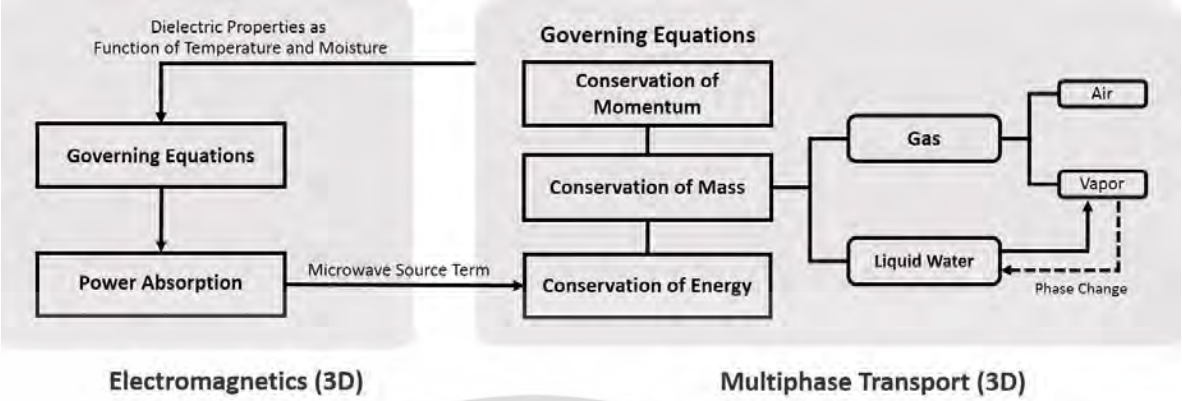

Figure 3.9 Flow chart of the sequence of steps followed to develop the computational model.

3.3.2.2.8 Model validation

In this study, the simulated average moisture content and temperature profiles were compared with the data collected from the experiment to validate the simulation results. The coefficient of determination (R-squared; R^2) was used to determine the accuracy of the simulation results, a value above 0.75 was only accepted.

Table 3.4 Additional input parameters used in the simulations.

Parameter	Value	Unit	Source
Specific heat			
- Water	4187	J/kg K	(Carr et al., 2013; Kumar et al., 2016)
- Vapor	1900	J/kg K	(Carr et al., 2013; Kumar et al., 2016)
- Air	1005.683	J/kg K	(Carr et al., 2013; Kumar et al., 2016)
Density			
- Water	1000	kg/m^3	(Datta, 2007; Kumar et al., 2016)
- Vapor	Ideal gas law	kg/m^3	(Kumar et al., 2016; Rakesh et al., 2012)
- Air	Ideal gas law	kg/m^3	(Kumar et al., 2016; Rakesh et al., 2012)
Thermal conductivity			
- Water	0.644	W/m K	(Datta, 2007; Kumar et al., 2016; Rakesh et al., 2012)
- Gas	0.026	W/m K	(Datta, 2007; Kumar et al., 2016; Rakesh et al., 2012)
Initial Equivalent porosity			
- Unripe banana	0.75	-	(Ni et al., 1999)
- Ripe banana	0.83	-	(Ni, 1997)
Initial water saturation			
- Unripe banana	0.5	-	(Ni et al., 1999)
- Ripe banana	0.8	-	(Ni, 1997)

Table 3.4 Additional input parameters used in the simulations (Cont'd).

Parameter	Value	Unit	Source
Intrinsic permeability			
Water	5×10^{-14}	m^2	(Ni et al., 1999; Rakesh et al., 2012)
Vapor and air	10×10^{-14}	m^2	(Ni et al., 1999; Rakesh et al., 2012)
Heat transfer coefficient	20	$W/m^2\ K$	(Ni et al., 1999)
Mass transfer coefficient	0.01	m/s	(Ni et al., 1999)
Binary diffusivity	2×10^{-6}	m^2/s	(Kumar et al., 2016; Rakesh et al., 2012)
Latent heat of evaporation	2.26×10^{6}	J/kg	(Çengal & Boles, 2011; Kumar et al., 2016; Rakesh et al., 2012)
Molecular weight of gas	28.966	g/mol	(Çengal & Boles, 2011; Kumar et al., 2016)
Molecular weight of vapor	18.016	g/mol	(Çengal & Boles, 2011; Kumar et al., 2016)
Molecular weight of water	18.016	g/mol	(Çengal & Boles, 2011; Kumar et al., 2016)
Universal gas constant	8.314	$J/mol\ K$	(Çengal & Boles, 2011; Kumar et al., 2016)
Ambient pressure	101325	Pa	(Çengal & Boles, 2011; Kumar et al., 2016; Rakesh et al., 2012)

CHAPTER 4

RESULTS AND DISCUSSION

4.1 FE model of temperature profiles of banana during microwave heating process

4.1.1 Experimental validation of temperature profiles

4.1.1.1 FE model of temperature profiles of banana at different ripening stages

Figure 4.1 shows the simulated temperature profiles of the unripe and ripe bananas during microwave heating compared with the experimental results, at various distances from the center of the sample. It is apparent that the agreement between the results of the simulation and the experiments was qualitatively consistent with R-squared values of unripe and ripe bananas were calculated as 0.9685 and 0.9815, respectively. Thus, this simulation can be considered sufficiently reliable to predict the temperature profiles.

4.1.1.2 FE model of temperature profiles of banana with different shapes

The simulated temperature profiles of two different shapes of banana are shown in Figure 4.2. The simulated temperature profiles were calculated R-squared which values are 0.9822 and 0.9764 for transversal and longitudinal, respectively. These values indicate that the simulation model can predict the temperature profiles with a reasonable accuracy.

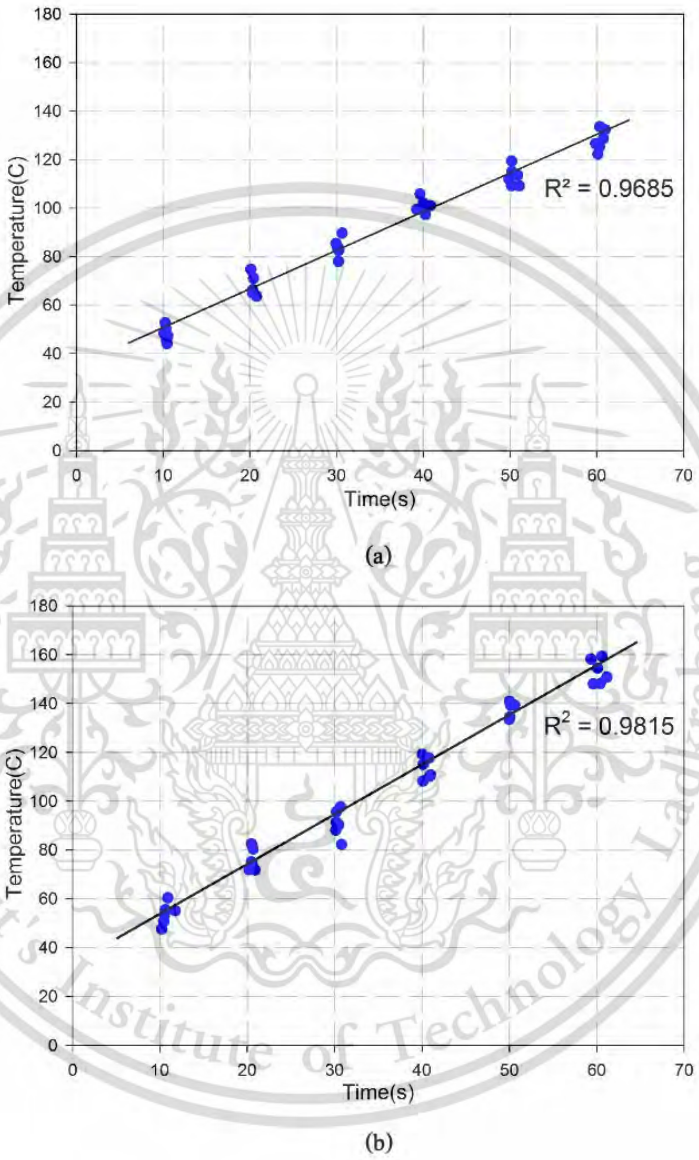

Figure 4.1 The temperature profile comparison between experiment and simulation; (a) unripe bananas; (b) ripe bananas.

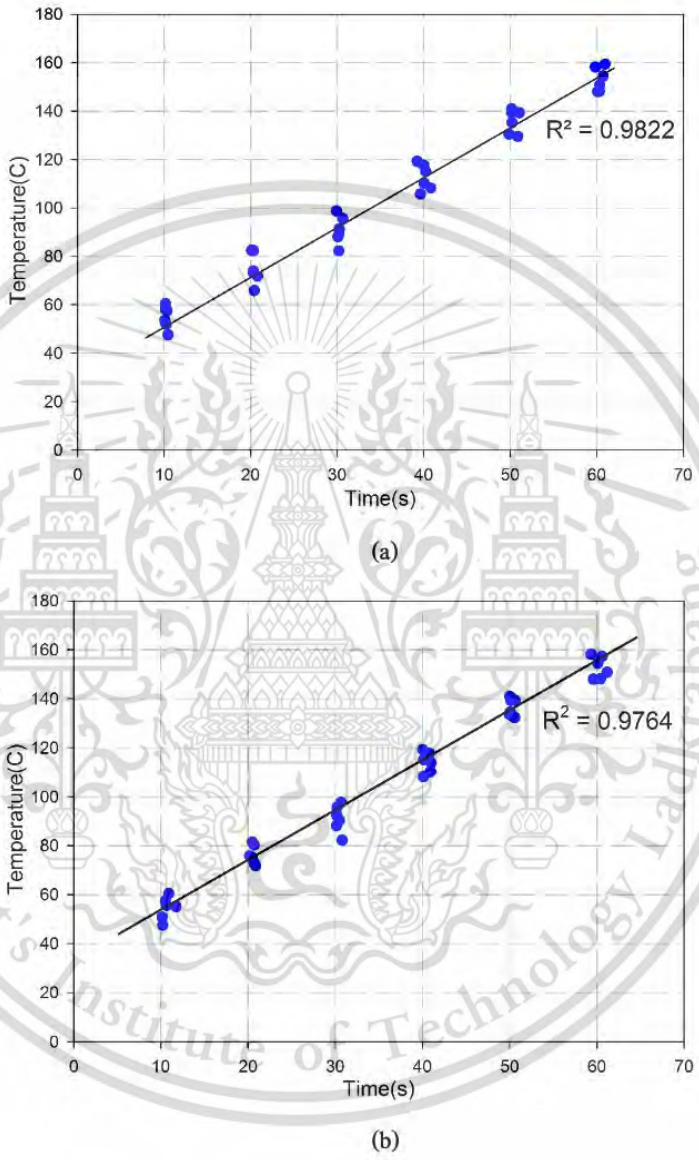

Figure 4.2 The temperature profile comparison between experiment and simulation; (a) transversal; (b) longitudinal.

4.2 The effect of ripening stages of banana on temperature profiles during microwave heating process based on FE model

Figure 4.3 shows the simulated temperature profiles of the unripe and ripe bananas during microwave heating. Both unripe and ripe bananas show similar patterns of non-uniform temperature distributions in their temperature profiles which the internal temperature was higher than the external temperature, the highest temperature was found at the center of the sample. In addition, the rate of increase in temperature of all time of unripe bananas is relatively slow in comparison to that observed in ripe bananas.

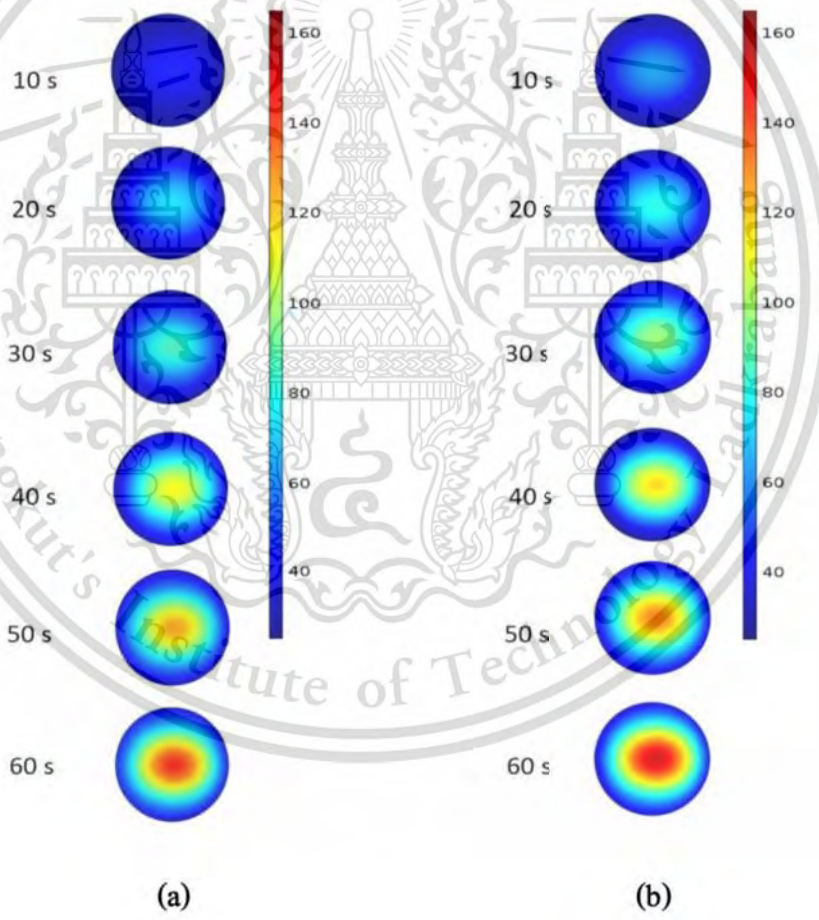

Figure 4.3 The simulation model of temperature profiles at different time intervals; (a) unripe bananas; (b) ripe bananas.

4.3 The effect of shapes of banana on temperature profiles during microwave heating process based on FE model

The simulated temperature profiles of two different shapes (transversal and longitudinal) of banana are shown in Figure 4.4. Both shapes show similar patterns of non-uniform temperature distributions, the internal temperature was higher than the external temperature. In addition, the heat was generated at center and distributed along the radius, hence the highest temperature was found at the center of both samples.

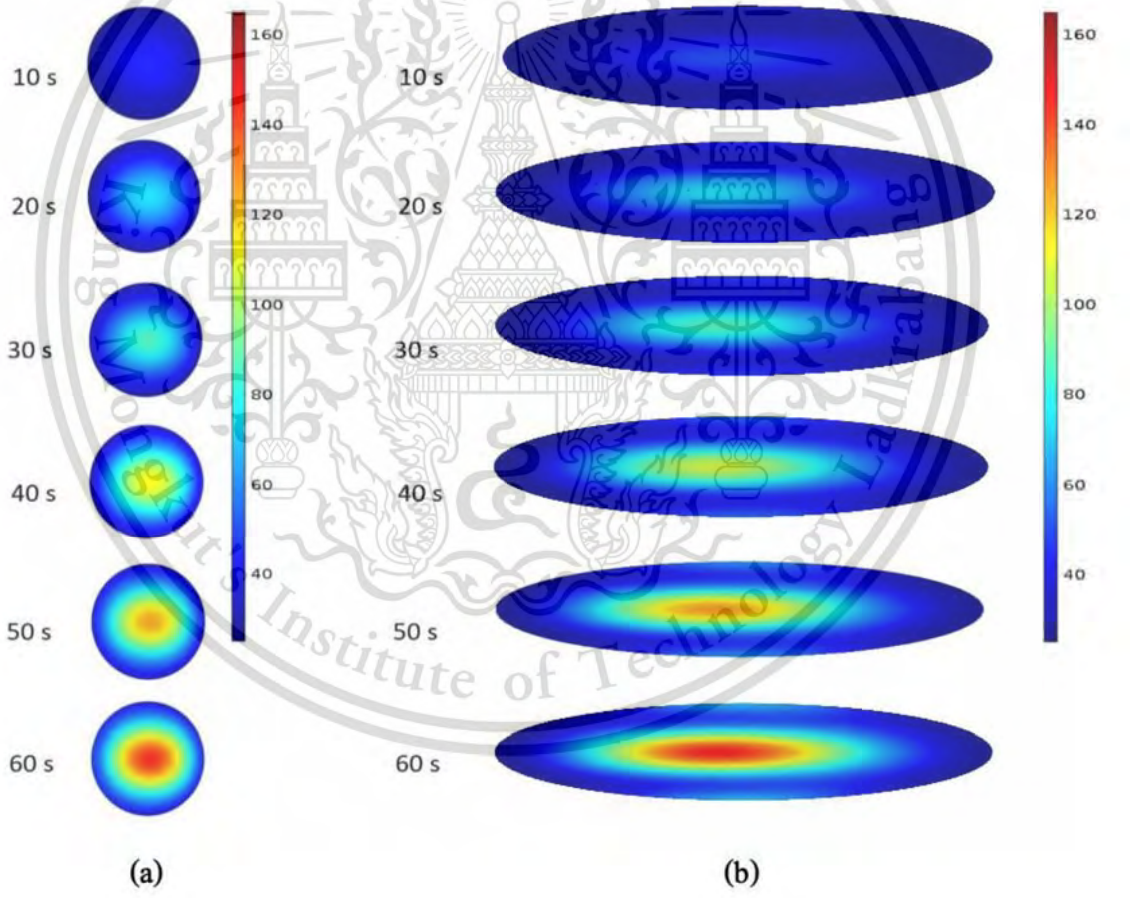

Figure 4.4 The simulation model of temperature profiles of banana at different time intervals; (a) transversal; (b) longitudinal.

Considering Figure 4.4, the average temperatures at cold and hot spots of unripe bananas were found to be 60 ℃ and 140 ℃, respectively. Meanwhile, the average temperatures at cold and hot spots of ripe bananas corresponded to 65 ℃ and 160 ℃, respectively.

According to the hot spot occurrence is influenced by the electromagnetic and thermodynamic features of the microwave system and the material (Kelen et al., 2006; Bizzi et al., 2011). The geometry of the material affects the heat distribution during microwave heating due to the penetration depth of the material. The penetration depth can be measured by the electromagnetic radiation that penetrates into a material. If the penetration depth is minor compared with the dimensions of the material, most of the energy is absorbed near the surface, leaving the center cold. Conversely, if the penetration depth is significant, reasonable amounts of energy reach the center and focusing occurs (Ryynänen, 2002; Pakdee & Rattanadecho, 2011).

The penetration depth can be given as (Pakdee & Rattanadecho, 2011)

$$d_p = \frac{\lambda}{2\pi} \cdot \left[\frac{2}{\varepsilon' \left(\sqrt{1 + tan^2\delta} - 1 \right)} \right]^{1/2} \quad \text{(Eq. 36)}$$

where d_p is the penetration depth in the material (mm); λ is the wavelength (m), and $tan\,\delta$ is the dielectric loss tangent, which is given by (Pakdee & Rattanadecho, 2011)

$$tan\,\delta = \frac{\varepsilon''}{\varepsilon'} \quad \text{(Eq. 37)}$$

Calculated by (Eq. 36), the penetration depth of a banana sample is 8.37 mm, due to the fact that the thickness of both transversal and longitudinal banana samples was set as 5 mm, which is less than the penetration depth. Therefore, the results are in agreement with those mentioned above in that most of the energy reaches to the center and focusing occurs; as a result, the hot spot was generated (Ryynänen, 2002; Pakdee & Rattanadecho, 2011). Chandrasekaran et al. (2013) also found that hot spots occur at the center for slab-shaped samples.

In addition, at the location of the hot spot, the temperature may be too high, which would cause overheating of the material or damage the nutrients' substance. In contrast, at the cold spot, the low temperature may fail to reach the damage temperature of the microorganisms, which would raise the risk of food deterioration (Chandrasekaran et al., 2013; Zhang et al., 2018). Thus, the cold and hot spots are very important to the design of the optimum process of microwave heating.

4.4 The phenomena of heat and moisture transport in bananas during microwave heating process based on FE model

4.4.1 Experimental validation of moisture content

During heating, the moisture content continually decreased due to the evaporation of water. As shown in Figure 4.5, the simulation model showed good agreement with the experiment, in which the R-squared values were 0.9733 for unripe bananas and 0.9721 for ripe bananas. Both the experiment and the simulation model showed that the average moisture content of samples after the end of the process at 60 s decreased from 45% wb to 5% wb for unripe bananas and 65% wb to 15% wb for ripe bananas.

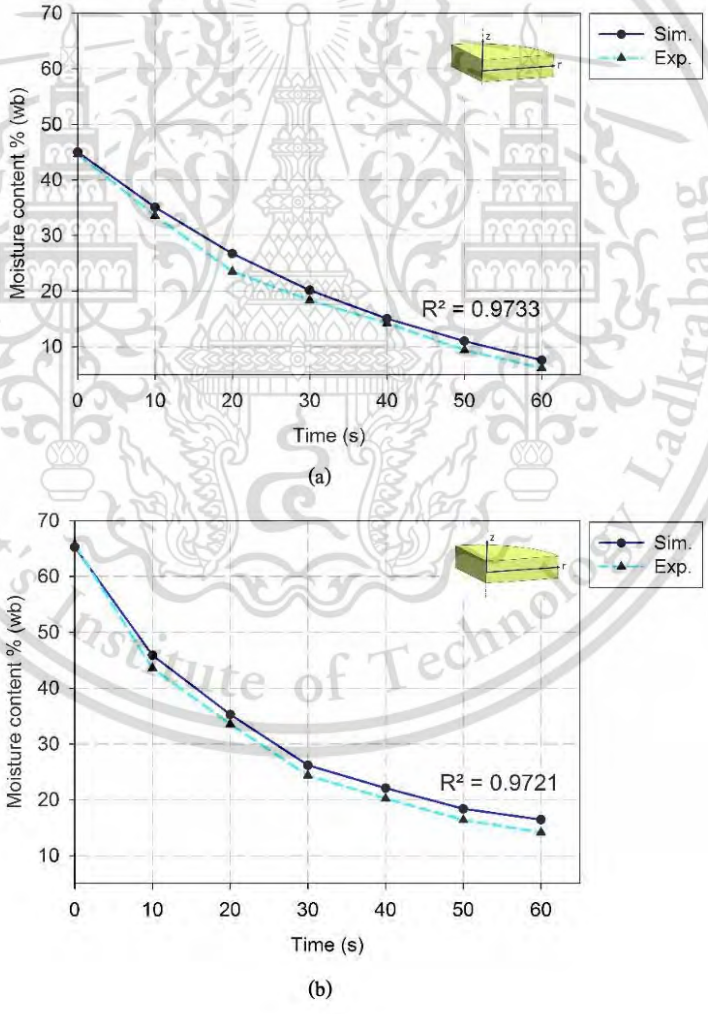

Figure 4.5 Comparison between predicted and experimental values of average moisture content of the sample during dehydration; (a) unripe bananas; (b) ripe bananas.

4.4.2 Experimental validation of temperature profiles

Figure 4.6 shows the simulated temperature profiles of the unripe and ripe bananas during microwave heating compared with the experimental results, at various distances from the center of the sample. It is apparent that the agreement between the results of the simulation and the experiments was qualitatively consistent. Additionally, this simulation can be considered sufficiently reliable to predict the temperature profiles of unripe and ripe bananas, due to the fact that the R-squared values of the simulated temperature profiles were calculated as 0.9778 and 0.9804, respectively.

Considering the results as shown in Figure 4.7, the temperature was plotted for the distance from the left to the right edge of the sample, at intervals of 10 s. This allows the investigation of temperature evolution both externally and internally with regard to the sample. Both unripe and ripe bananas show similar patterns of non-uniform temperature distributions: the temperature peaked at the center, where a hot spot was observed. The surface region of the sample, in contrast, remains cools because the air surrounding the food is able to exert a cooling influence (Suwannapum & Rattanadecho, 2011). While the internal temperature increases continually with heating time and is distributed from the center to the surface, the surface has a lower temperature, resulting from evaporative cooling (Suwannapum & Rattanadecho, 2011).

In comparing the unripe and ripe bananas, unripe bananas (Figure 4.7a), the rate of increase in temperature over time is relatively slow in comparison to that observed in ripe bananas (Figure 4.7b) with the range of simulated temperatures for the unripe and ripe bananas from the start to the end of the heating process was about 25–140 ℃ and 25–160 ℃, respectively. The highest temperatures, which were found at the centers of the samples, were about 140 ℃ for unripe and 160 ℃ for ripe bananas.

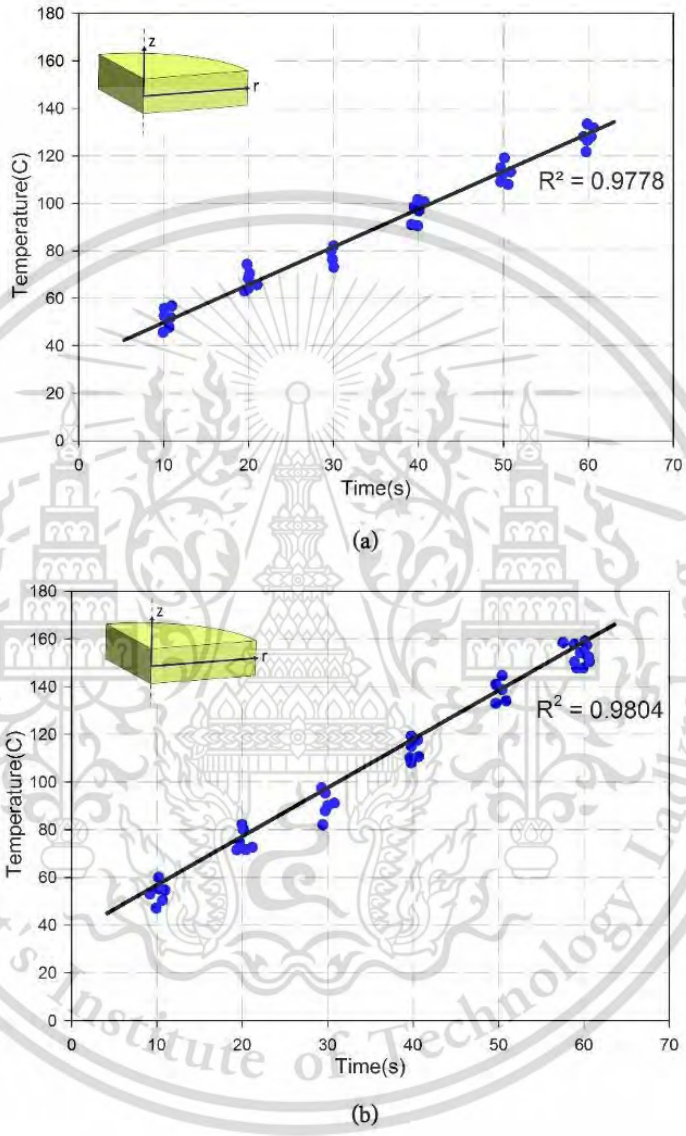

Figure 4.6 The temperature profile comparison between experiment and simulation; (a) unripe bananas; (b) ripe bananas.

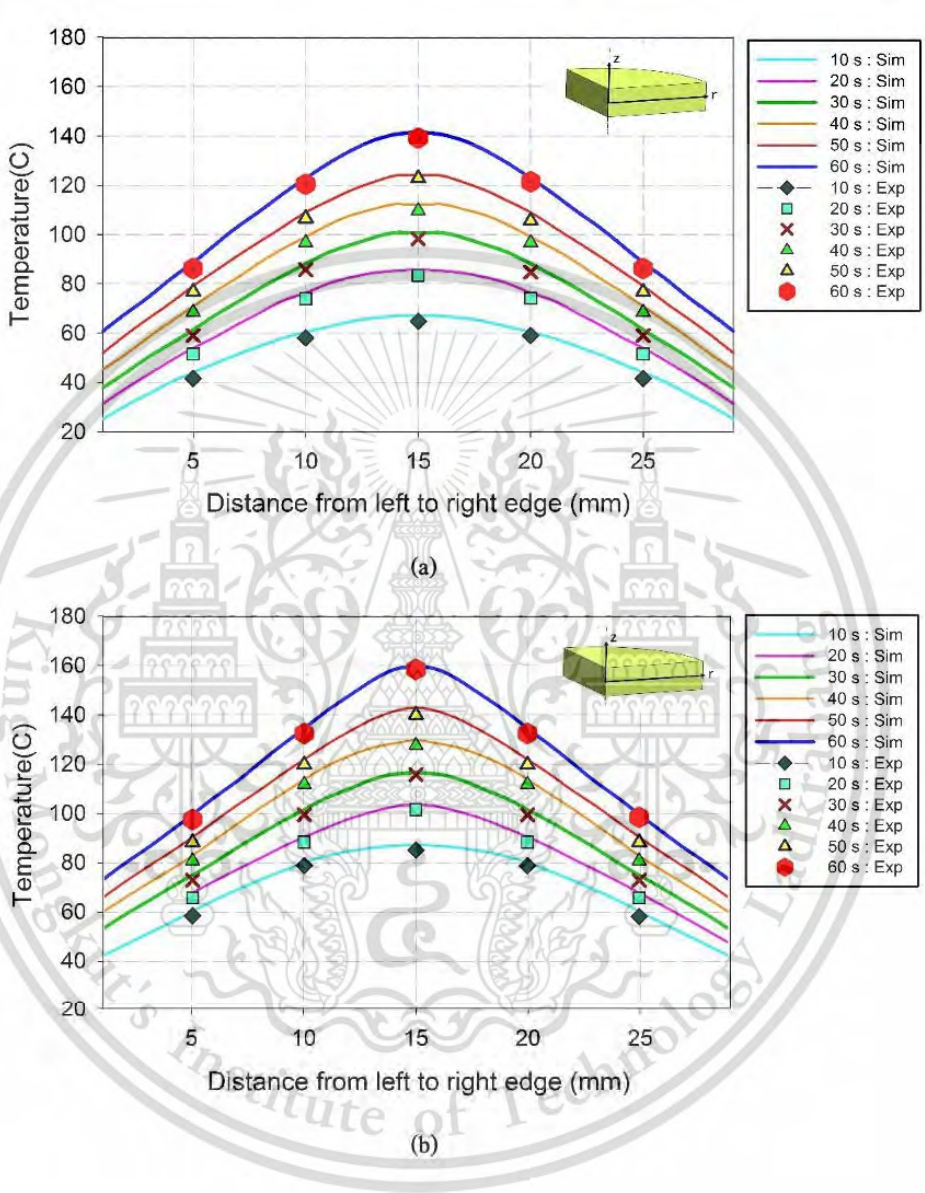

Figure 4.7 Temperature at different distances;

(a) unripe bananas; (b) ripe bananas.

4.4.3 The moisture profiles

Distance-dependent changes in the water saturation profiles of bananas during dehydration are shown in Figure 4.8. Both unripe and ripe bananas had similar water saturation profiles, in which there were high moisture saturation regions at the center, toward 10 mm in the radial direction; and the moisture saturation sharply decreased from 10 mm to the surface of the banana at 15 mm in the radial direction. This result indicates that a higher moisture content exists in the center than on the surface during heating, due to the fact that the liquid water that migrates from the internal part of the sample to the surface is transformed to vapor and vaporizes from the surface to the surroundings (Chen et al., 2001; Ratanadecho et al., 2002; Khan et al., 2018); accordingly, there is a lower moisture content at the surface. In addition, it can be seen that at the central region, the water saturation at the end of the process decreased slightly due to a lower rate of evaporation, when compared with the surface region. After heating for 60 s, the water saturation at the center of the sample dropped from 0.5 to 0.45 for unripe bananas and 0.8 to 0.76 for ripe bananas. Mercier et al. (2014) and Kumar et al. (2016) also found this phenomenon.

4.4.4 The vapor mass fraction profiles

The vapor mass fractions at various time intervals are shown in Figure 4.9. Both unripe and ripe bananas show similar results, in which the vapor mass fraction decreases gradually with distance from the center up to 10 mm from the center. A higher decreasing rate of mass fraction was revealed around the surface region, and a higher gradient profile developed along with the increasing time steps. The vapor mass fraction increases with time, at any distance, because of moisture evaporation in correspondence with the raising temperature. The highest vapor mass fraction occurs at the center of the sample. Vapor mass fractions correlate with the temperature profiles. The higher vapor mass fractions are found in the regions where the high temperatures are found, at any time interval during the dehydration process. This was due to the internal region having a greater rate of moisture evaporation than moisture transport to the surface region. For this reason, the lower vapor mass fractions occur at the surface due to the transportation of moisture to the surrounding or ambient air (Kumar et al., 2016). Again, due to the lower initial moisture content of unripe bananas, the vapor mass fraction is also lower than that of ripe bananas at the same time interval.

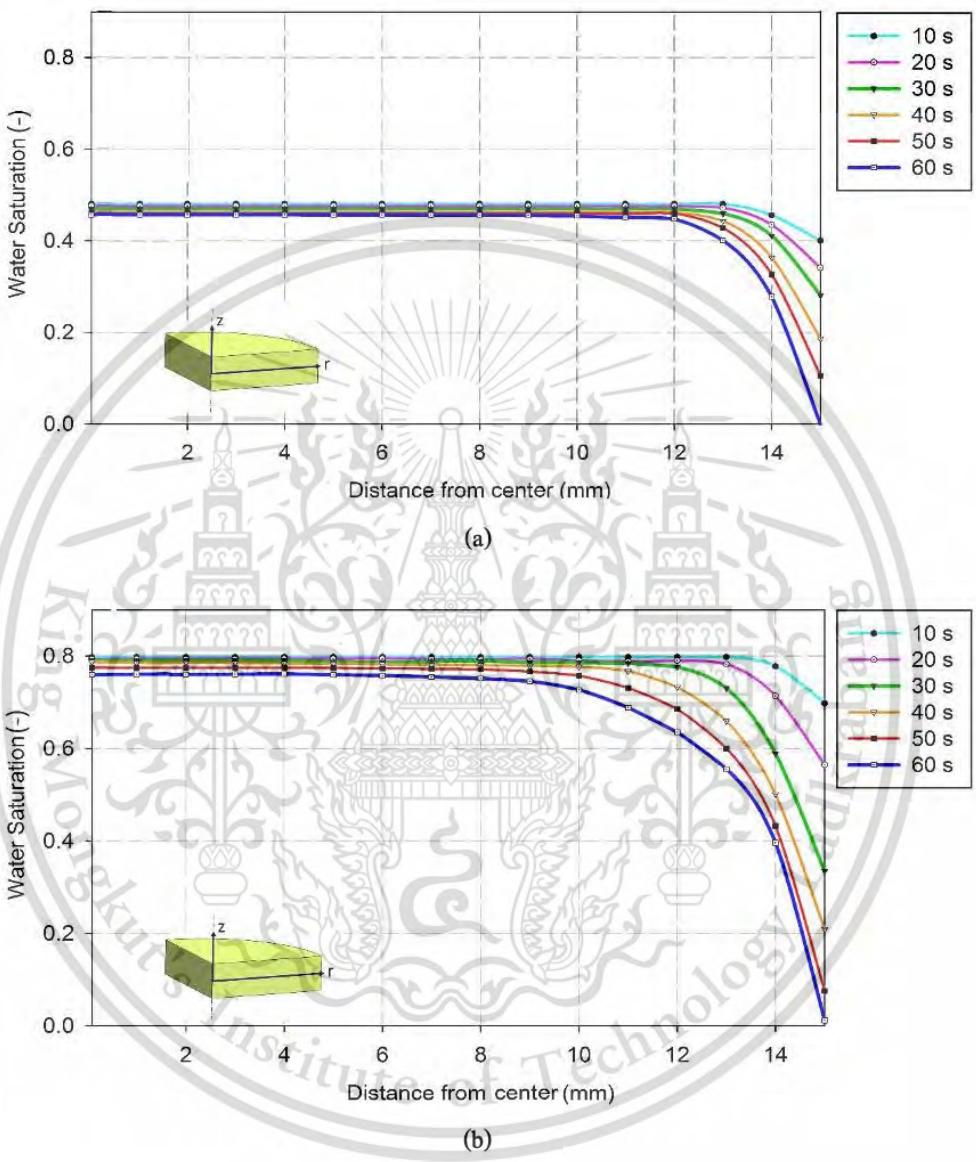

Figure 4.8 The water saturation profiles;

(a) unripe bananas; and (b) ripe bananas.

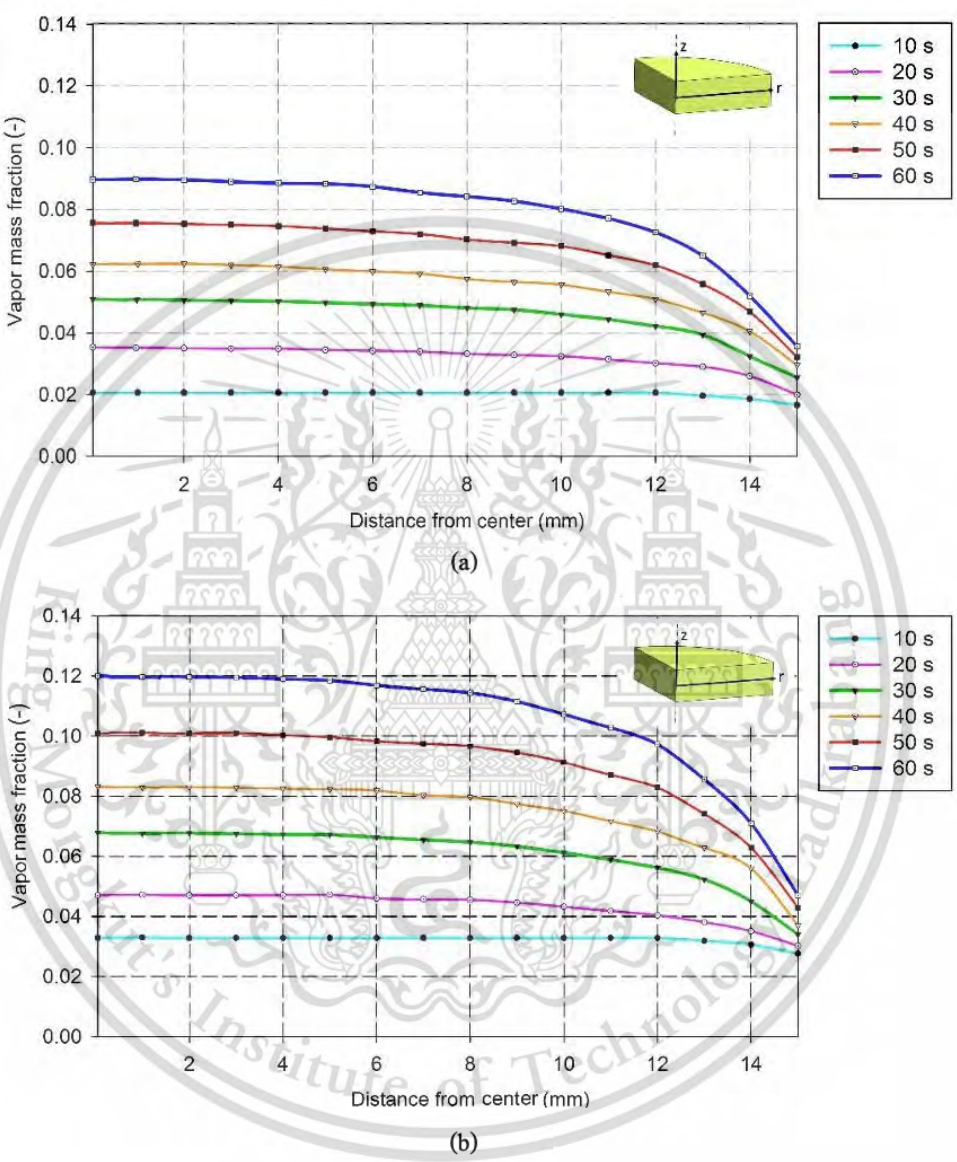

Figure 4.9 The vapor mass fractions profiles;

(a) unripe bananas; and (b) ripe bananas.

4.4.5 The vapor pressure profiles

The vapor pressure profiles within the banana samples at each time interval are shown in Figure 4.10. The results show that for both unripe and ripe bananas, the vapor pressure is higher at the internal region of the sample, with the highest vapor pressure occurring at the center. The unripe bananas have lower vapor pressure levels compared with the ripe bananas at the same time interval. These behaviors of vapor pressure are similar to the moisture and vapor mass fraction profiles, which correlate with the temperature profiles.

Halder et al. (2007) found a similar result to our study in that at the beginning of heating, vapor pressure in the core region was lower, which was caused by the condensation of migrated water and vapor from the surface to the internal region. However, when the evaporation of moisture increased as temperature rose in the center region, then vapor saturation in the region rose, which led to an increase in vapor pressure, which pushed the vapor flow through the porous medium toward the surface (Khan et al., 2018). In addition, on the surface of the material, where vapor pressure was close to ambient pressure, the vapor could be readily diffused into the surrounding air, allowing the surface to dry (Thorvaldsson & Janestad, 1999; Kumar et al., 2016).

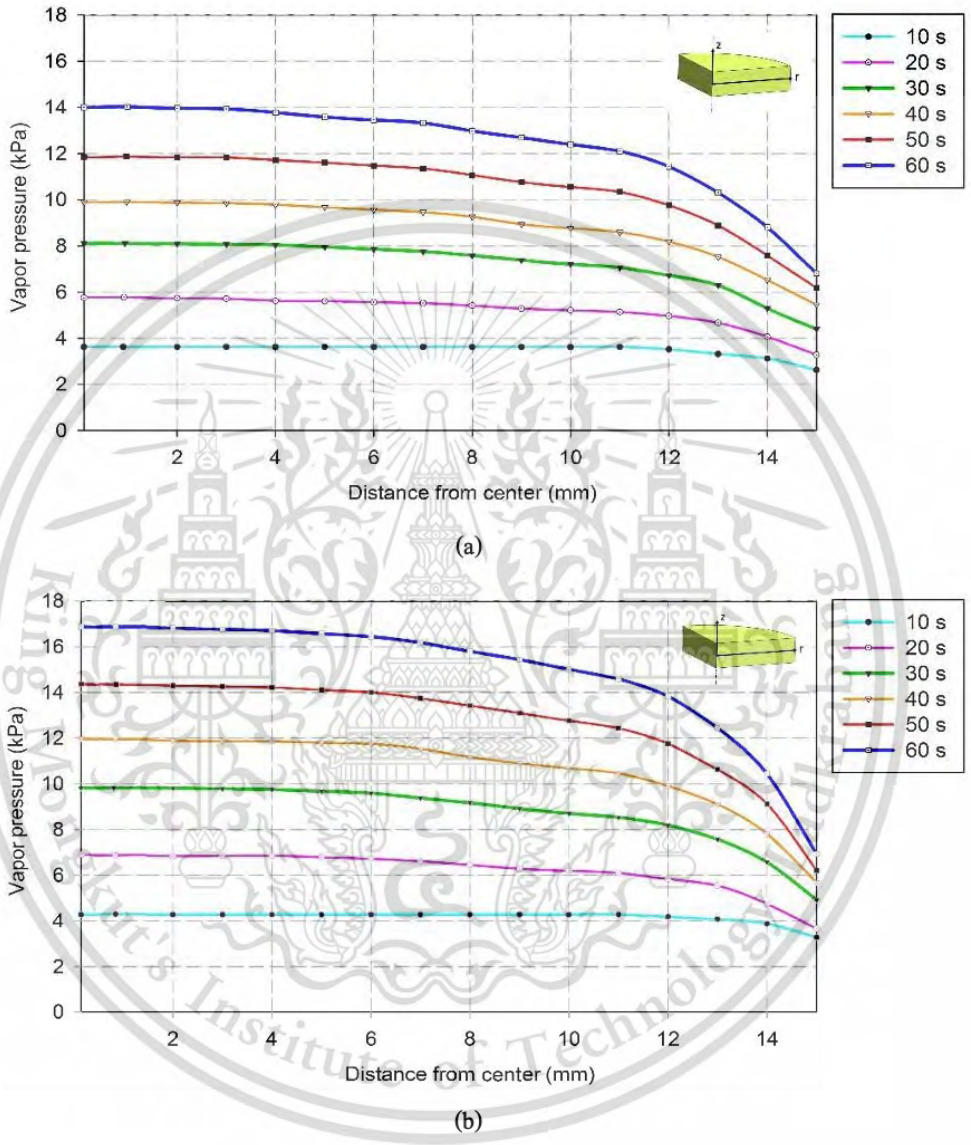

Figure 4.10 The vapor pressure profiles;

(a) unripe bananas; and (b) ripe banana.

4.4.6 Vapor and water fluxes

Figures 4.11 and 4.12 show the liquid water fluxes due to the capillary diffusion and gas pressure gradient of the banana, respectively. It can be seen that both the liquid water fluxes show results with quite similar patterns, in which the liquid water fluxes decrease over time. The higher liquid water fluxes occur near the surface region, while the liquid water fluxes decrease at the internal regions towards the center, with the lowest value occurring at the center. The peaks of the fluxes are found at small distances from the surface. This could be due to the fact that at the surface, the moisture is higher, because the external region close to the surface has less moisture and hence the concentration gradient is higher, which leads to greater fluxes (Kumar et al., 2016).

It can be seen that the vapor flux due to the binary diffusion of the banana (Figure 4.13) and the vapor flux due to gas pressure (Figure 4.14) have similar profile patterns. The figures show that both of these vapor fluxes increase over the heating time, and sharply increase at about 10 mm from the center, with the highest fluxes occurring at the surface. With time, it can also be seen that both of these vapor fluxes move slightly towards the internal region. However, these slight changes are insignificant in distance, and both vapor fluxes still occur at or near the surface. As a result, due to the gradient of the vapor being very high near the surface, higher diffusive flux is caused, along with more moisture loss (Kumar et al., 2016).

Unripe and ripe bananas show similar profile patterns in both water and vapor flux. However, due to the initial moisture content, a slight difference can be seen in the levels of fluxes at the same time interval.

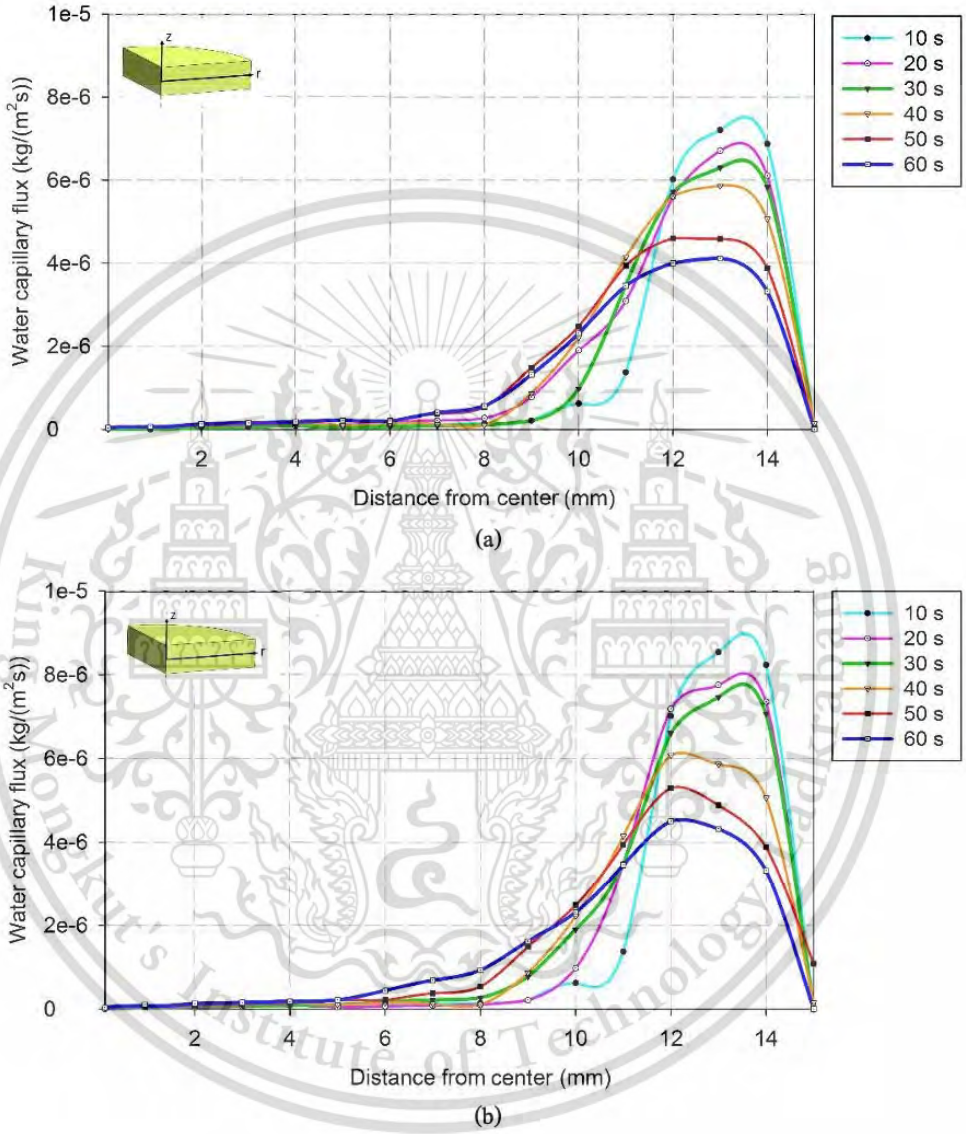

Figure 4.11 Water flux due to capillary;

(a) unripe bananas; and (b) ripe bananas.

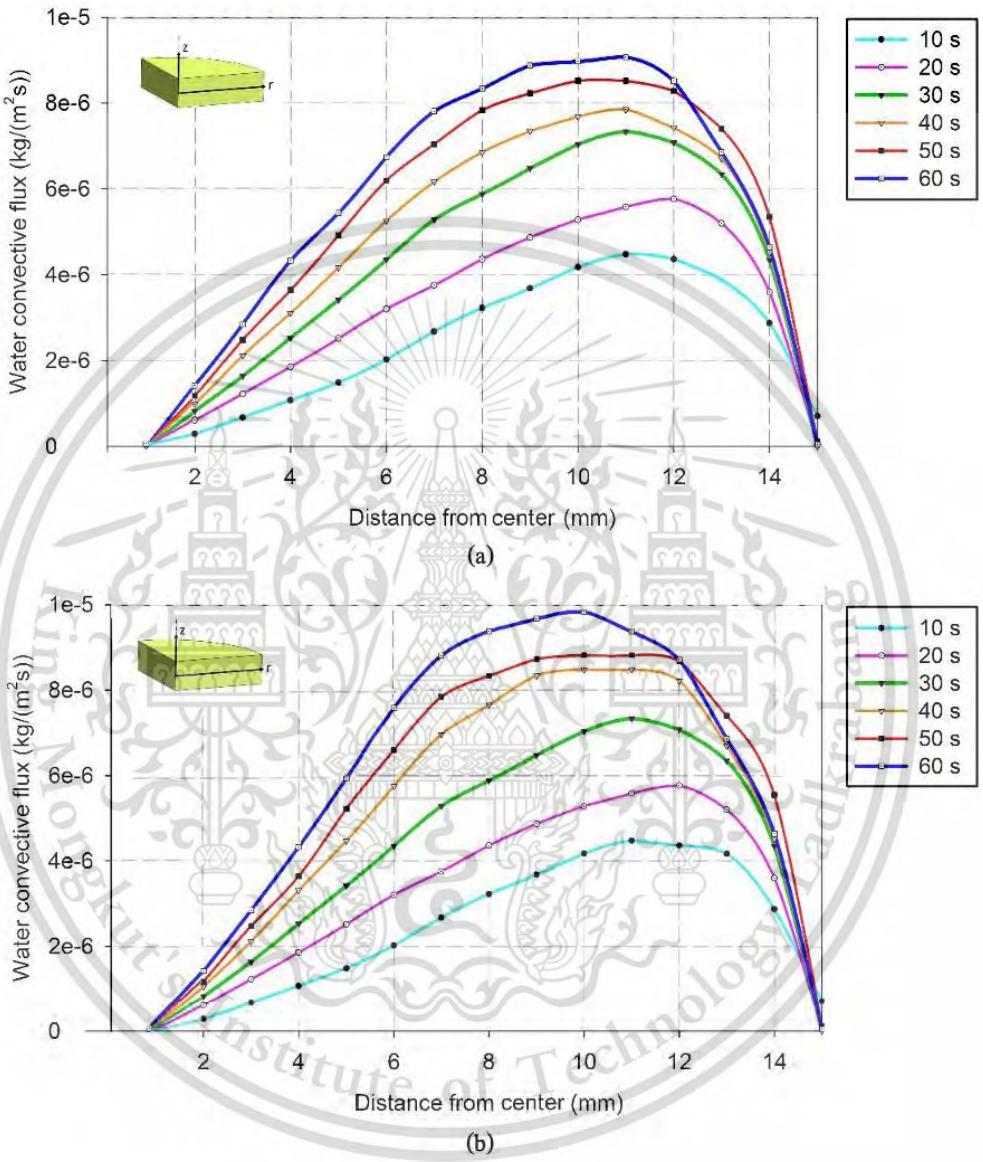

Figure 4.12 Water flux due to gas pressure;

(a) unripe bananas; and (b) ripe bananas.

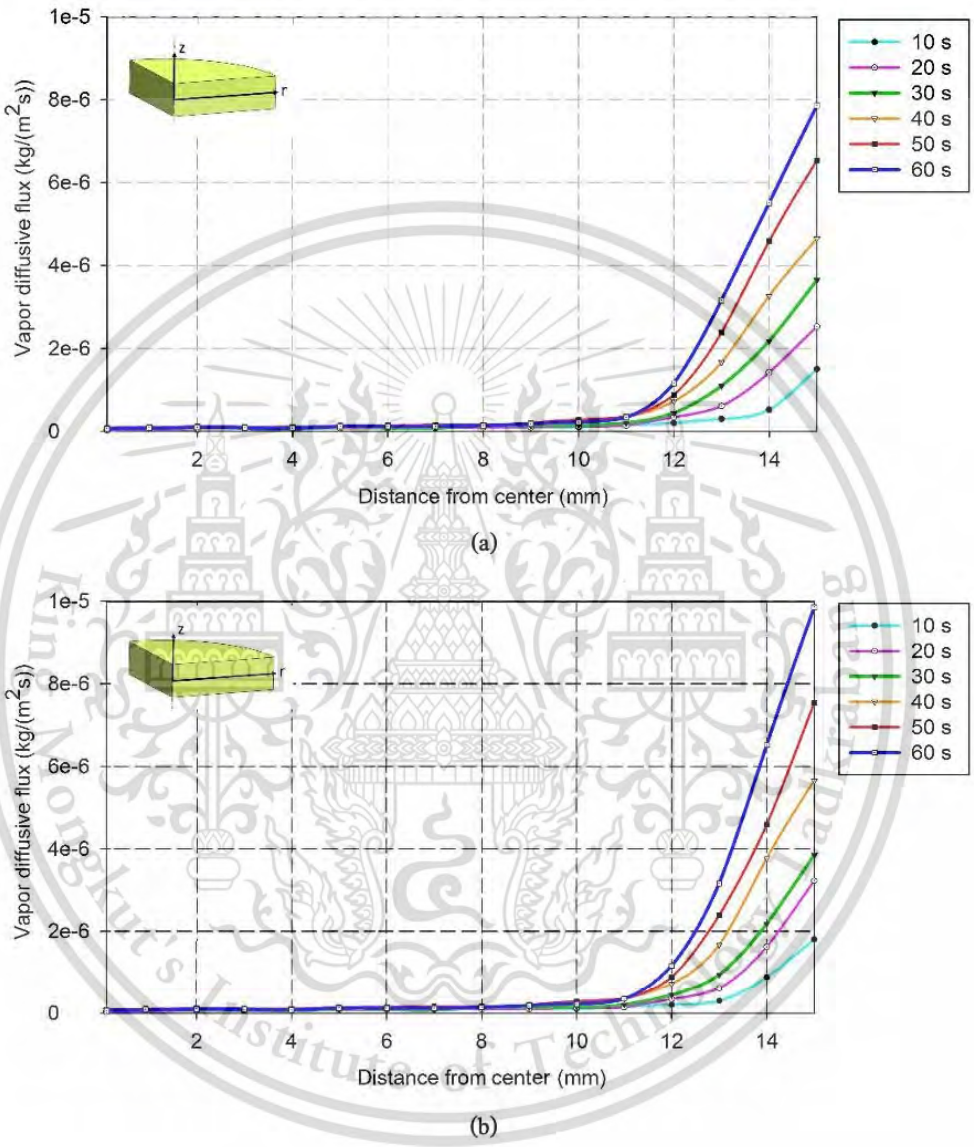

Figure 4.13 Vapor flux due to binary diffusion;

(a) unripe bananas and, (b) ripe bananas.

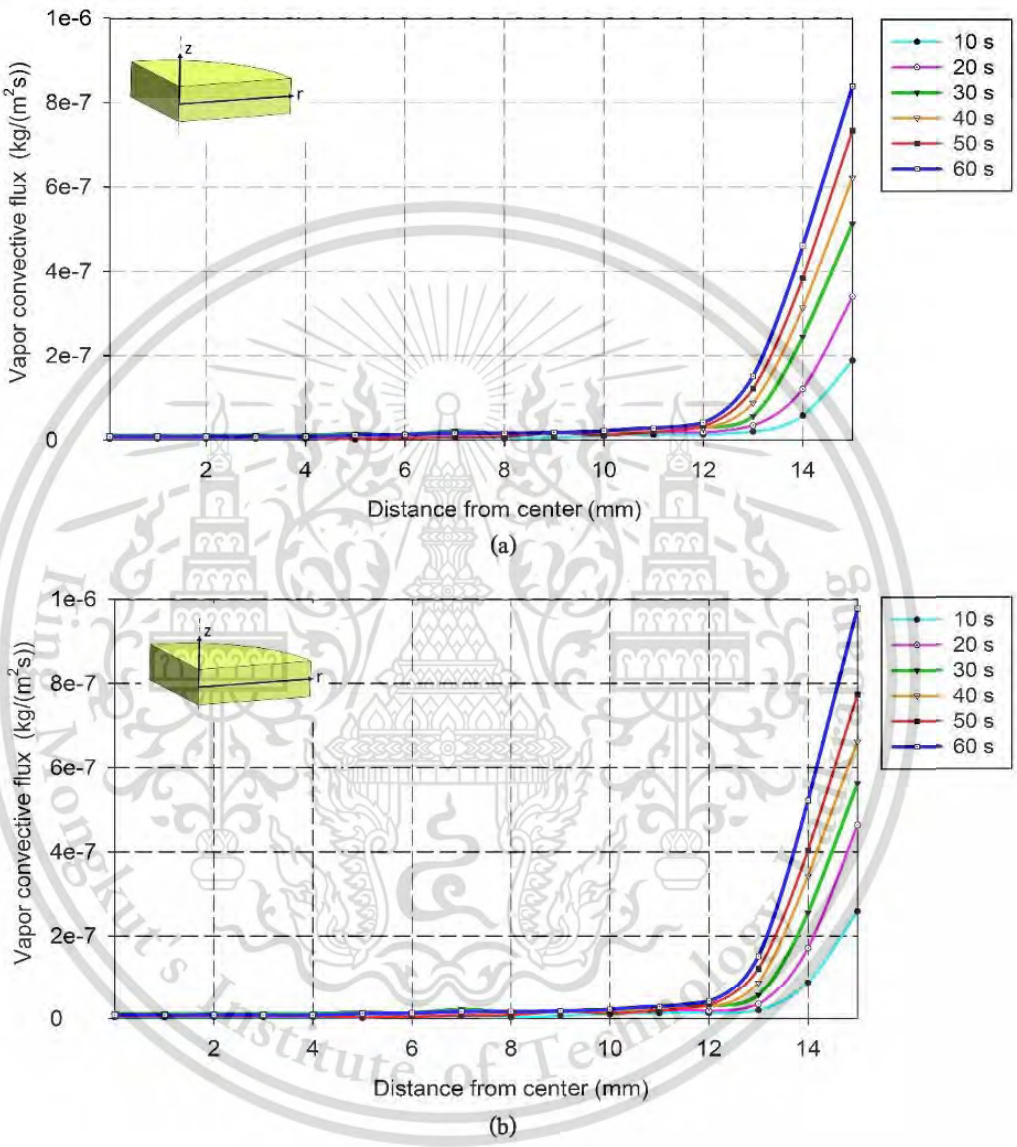

Figure 4.14 Vapor flux due to gas pressure;

(a) unripe bananas and, (b) ripe bananas.

4.4.7 Comparison of unripe and ripe bananas

As can be seen in Figure 4.7a, unripe bananas as a low moisture material had a fairly slow temperature increase, since the rate of the microwave absorption was lower due to its low moisture content. At about 10 s of heating time, the first signs of heat generation at the center of the sample could be clearly seen, and it reached 100 ℃ at about 30 s. As the temperature increased, the rate of evaporation also increased, and the internal pressure started to build up. Thus, the lower internal temperatures caused a lower rate of evaporation and lower pressure generation. This process created a pressure gradient, which caused a fast movement of the liquid water and water vapor towards the surface of the material.

Ripe bananas with high initial moisture content were considered as high moisture material, as under the same heating condition, the patterns of the temperature, moisture, and pressure profiles were similar to those of unripe bananas. However, ripe bananas showed a slight elevation in the level of values, as can be seen in Figure 4.7b. The temperature profiles of ripe bananas could reach 100 ℃ at the center of the sample at about 20 s, faster than unripe bananas. With temperature dependence, the higher internal temperatures caused a higher rate of evaporation and higher pressure generation; consequently, the heating rate was also higher than that in the low moisture material of unripe bananas.

Therefore, the sorting or grading of bananas into the correct ripening stages was an important process to achieve the optimum process for the dehydration of bananas by microwave heating. This was due to the differences in initial moisture content, which could generate different microwave absorption profiles, causing a difference in the dehydration phenomenon as well.

CHAPTER 5

CONCLUSIONS

5.1 Conclusions

As the objectives of this study were to establish a FE model to study the temperature profiles of banana during microwave heating process which can demonstrate the effects of ripening stages and shapes of banana on temperature profiles and investigate the phenomena of heat and moisture transport in bananas during the process. The conclusions are summarized as follows:

5.1.1 A model for prediction temperature profiles of banana during microwave heating based on the FEM was established. The simulated results correlated well with the experimental results, considered sufficiently reliable.

5.1.2 The temperature distribution profiles of both unripe and ripe banana samples are non-uniform. The heat generated at the center of the sample, then distributed to external regions, also the temperature rapidly increased with time. The rate of increase in temperature of all time of unripe bananas is relatively slow in comparison to that observed in ripe bananas.

5.1.3 Both transversal and longitudinal shapes of banana slices show similar patterns of non-uniform temperature profiles. The heat generated at the center of the sample and distributed along the radius. The heat remains focused at the center of all time due to their minimum thickness, which is less than the penetration depth, the hot spot was found.

5.1.4 The moisture, vapor, and pressure distribution profiles showed similar phenomena, which correlated with the temperature distribution profiles. High temperatures caused moisture immigration and the phase transition of water within the sample. At the center, at the highest temperature point, the results showed that the water saturation, vapor mass fraction, and vapor pressure were higher than at the external regions due to the evaporation of the water affecting the water behavior within the sample. The water and vapor fluxes were also correlated with this water behavior. Both unripe and ripe banana samples showed similar patterns to each other, for all profiles. In comparing the unripe and ripe bananas, ripe bananas showed a slight elevation in the level of values than unripe bananas due to their initial moisture content.

5.2 Industrial relevance

In Thailand, the banana production plays a significant role to increase farm income and food security and sustainable. Bananas can be consumed raw, cooked or processed into many types of food products. However, overproduction of banana in the peak periods causes too-low prices. Furthermore, ripe bananas are regarded as highly perishable food due to their high moisture content. Thus, there is a need for dehydration of banana to reduce the losses which is to increase the dehydrated banana products through the development of food processing.

Conventional drying is commonly used to dry bananas in Thailand, but their textural properties are very poor because of high shrinkage of solid matrix and low porosity. Microwave heating process has been used as an alternative method of dehydration to obtain high quality dried banana due to this method has several advantages such as higher drying rate, shorter drying time, decreased energy consumption and better quality of the dried banana products when compared with the conventional drying. However, the major drawback of microwave drying is its non-uniform heating, particularly the overheating at some location of the sample which depend on its shape, resulting in hot and cold spots which affect the quality of the food and raise the issue of food safety.

Understanding the effects of ripening stages and shapes of banana on temperature profiles and the phenomena of heat and moisture transport in bananas during the process are beneficial for the improvement, development, and design of the optimum process for dehydration in bananas with microwave heating. The identification of hot-spot and cold-spot regions can help to avoid the problem of overheated or undercooked areas, which degrade the quality of products and also result in a failure to reach the necessary temperatures to eliminate microorganisms, thereby raising the risk of food deterioration and foodborne illnesses.

Besides, the simulation eliminates the need to perform multiple experiments. There is no need to replicate conditions, and the process is sped up immeasurably. This allows research to be carried out quickly and at minimal cost.

REFERENCES

Abbott, J. A. (1999). Quality measurement of fruits and vegetables. *Postharvest biology and technology, 15*(3), 207-225.

Acevedo, L., Ferreira, G., & López-Sabirón, A. M. (2021). Exergy transfer principles of microwavable materials under electromagnetic effects. *Materials Today Communications, 27*, 102313.

Albuquerque, C. D. d., Curet, S., & Boillereaux, L. (2019). A 3D-CFD-heat-transfer-based model for the microbial inactivation of pasteurized food products. *Innovative Food Science & Emerging Technologies, 54*, 172-181.

Apinyavisit, K., Nathakaranakule, A., Mittal, G. S., & Soponronnarit, S. (2018). Heat and mass transfer properties of longan shrinking from a spherical to an irregular shape during drying. *Biosystems Engineering, 169*, 11-21.

Arvanitoyannis, I. S., Mavromatis, A. G., Grammatikaki-Avgeli, G., & Sakellariou, M. (2008). Banana: cultivars, biotechnological approaches and genetic transformation. *International Journal of Food Science & Technology, 43*(10), 1871-1879.

Aurore, G., Parfait, B., & Fahrasmane, L. (2009). Bananas, raw materials for making processed food products. *Trends in Food Science & Technology, 20*(2), 78-91.

Barba, A. A., & d'Amore, M. (2012). Relevance of dielectric properties in microwave assisted processes. *Microwave Materials Characterization, 6*, 91-118.

Basak, T., & Meenakshi, A. (2006). A theoretical analysis on microwave heating of food slabs attached with ceramic plates: Role of distributed microwave incidence. *Food Research International, 39*(8), 932-944.

Bello-Pérez, L. A., Agama-Acevedo, E., Osorio-Díaz, P., Utrilla-Coello, R. G., & García-Suárez, F. J. (2011). Chapter 22 - Banana and Mango Flours. In V. R. Preedy, R. R. Watson, & V. B. Patel (Eds.), *Flour and Breads and their Fortification in Health and Disease Prevention* (pp. 235-245). San Diego: Academic Press.

Bern, M. W., & Plassmann, P. E. (2000). Chapter 6 - Mesh Generation. In J.-R. Sack, & J. Urrutia (Eds.), *Handbook of computational geometry* (pp. 291-332). Boston: Elsevier.

Bianchi, C., Datta, A. K., & Dughiero, F. (2019). Mechanistic understanding of plasma arcing in microwave food processing. *Chemical Engineering Science, 195*, 141-158.

Bizzi, C. A., Barin, J. S., Hermes, A. L., Mortari, S. R., & Flores, É. M. (2011). A fast microwave-assisted procedure for loss on drying determination in saccharides. *Journal of the Brazilian Chemical Society, 22*(2), 376-381.

Boz, Z., Erdogdu, F., & Tutar, M. (2014). Effects of mesh refinement, time step size and numerical scheme on the computational modeling of temperature evolution during natural-convection heating. *Journal of Food Engineering, 123*, 8-16.

Brown, N., Venkatasamy, S., Khittoo, G., Bahorun, T., & Jawaheer, S. (2009). Evaluation of genetic diversity between 27 banana cultivars (*Musa* spp.) in Mauritius using RAPD markers. *African Journal of Biotechnology, 8*(9), 1834-1840.

Campañone, L. A., Bava, J. A., & Mascheroni, R. H. (2014). Modeling and process simulation of controlled microwave heating of foods by using of the resonance phenomenon. *Applied Thermal Engineering, 73*(1), 914-923.

Carr, E. J., Turner, I. W., & Perre, P. (2013). A dual-scale modeling approach for drying hygroscopic porous media. *Multiscale Modeling & Simulation, 11*(1), 362-384.

Caussiol, L. (2001). Postharvest quality of conventionally and organically grown banana fruit.

Çengal, Y., & Boles, M. A. (2011). Vapor and combined power cycles. *Thermodynamics an Engineering Approach*, 565-621.

Chandrasekaran, S., Ramanathan, S., & Basak, T. (2013). Microwave food processing—A review. *Food Research International, 52*(1), 243-261.

Chen, G., Wang, W., & Mujumdar, A. S. (2001). Theoretical study of microwave heating patterns on batch fluidized bed drying of porous material. *Chemical Engineering Science, 56*(24), 6823-6835.

Chen, J., Pitchai, K., Birla, S., Jones, D., Negahban, M., & Subbiah, J. (2016). Modeling heat and mass transport during microwave heating of frozen food rotating on a turntable. *Food and Bioproducts Processing, 99*, 116-127.

Cheng, A. H.-D., & Cheng, D. T. (2005). Heritage and early history of the boundary element method. *Engineering Analysis with Boundary Elements, 29*(3), 268-302.

Choudhary, A., Gopirajah, R., & Anandharamakrishnan, C. (2018). Computational modeling of dehydration of mushroom. *MOJ Food Process Technology, 6*(3), 264-270.

COMSOL (2015). *RF module user's guide*. COMSOL Multiphysics® Version 5.2., Stockholm: COMSOL AB.

CSIRO (1972). *Banana Ripening Guide*. North Ryde, NSW: Commonwealth Scientific Industrial Research Organisation Division of Fruit Research.

Datta, A. (2007). Porous media approaches to studying simultaneous heat and mass transfer in food processes. II: Property data and representative results. *Journal of Food Engineering, 80*(1), 96-110.

Dixit, U. S. (2007). Finite element method: an introduction. *Indian Institute of Technology Guwahati-781, 39*.

Doymaz, İ. (2010). Evaluation of mathematical models for prediction of thin-layer drying of banana slices. *International Journal of Food Properties, 13*(3), 486-497.

Duan, X., Cheng, G., Yang, E., Yi, C., Ruenroengklin, N., Lu, W., Lou, Y., & Jiang, Y. (2008). Modification of pectin polysaccharides during ripening of postharvest banana fruit. *Food Chemistry, 111*(1), 144-149.

Durance, T., & Yaghmaee, P. (2011). Chapter 4.51 - Microwave dehydration of food and food ingredients. In M. Moo-Young (Ed.), *Comprehensive biotechnology* (pp. 617-628). Boston: Elsevier.

Ernens, D. (2011). *Finite element methods with exact geometry representation* (Master's Thesis). Delft University of Technology, Delft, Netherlands.

Esveld, E., Bows, J., Vollebregt, M., & van der Sman, R. (2018). In-situ Single Mode Dielectric Measurements of microwaveable snack pellets. *Journal of Food Engineering, 231*, 109-122.

Felippa, C. A. (2004). Chapter 6 - Finite Element Modeling: Introduction. In C. A. Felippa (Ed.), *Introduction to Finite Element Methods* (pp. 6.1-6.15). Colorado: University of Colorado.

Gao, X., Liu, X., Yan, P., Li, X., & Li, H. (2019). Numerical analysis and optimization of the microwave inductive heating performance of water film. *International Journal of Heat and Mass Transfer, 139,* 17-30.

Geedipalli, S., Rakesh, V., & Datta, A. (2007). Modeling the heating uniformity contributed by a rotating turntable in microwave ovens. *Journal of Food Engineering, 82*(3), 359-368.

Ghag, S. B., & Ganapathi, T. R. (2019). Banana and Plantains: Improvement, Nutrition, and Health. In J.-M. Mérillon & K. G. Ramawat (Eds.), *Bioactive Molecules in Food* (pp. 1-20). Cham: Springer.

Goulao, L. F., & Oliveira, C. M. (2008). Cell wall modifications during fruit ripening: when a fruit is not the fruit. *Trends in Food Science & Technology, 19*(1), 4-25.

Gulati, T., Zhu, H., & Datta, A. K. (2016). Coupled electromagnetics, multiphase transport and large deformation model for microwave drying. *Chemical Engineering Science, 156*, 206-228.

Hadagali, P. (2014). *Subject-specific finite element modeling of the adolescent thoracic spine for scoliosis research* (Master's Thesis). Drexel University, Pennsylvania, United States.

Halder, A., Dhall, A., & Datta, A. (2007). An improved, easily implementable, porous media based model for deep-fat frying: Part II: Results, validation and sensitivity analysis. *Food and Bioproducts Processing, 85*(3), 220-230.

Hazervazifeh, A., Nikbakht, A. M., & Nazari, S. (in press). Industrial microwave dryer: An effective design to reduce non-uniform heating. *Engineering in Agriculture, Environment and Food*.

Hosseini, M., Kaasinen, A., Link, G., Lähivaara, T., & Vauhkonen, M. (2020). LQR Control of Moisture Distribution in Microwave Drying Process Based on a Finite Element Model of Parabolic PDEs. *IFAC-PapersOnLine, 53*(2), 11470-11476.

Houšová, J., & Hoke, K. (2001). Temperature profiles in microwave heated solid foods of slab geometry: Influence of process parameters. *Czech Journal of Food Sciences, 19*(3), 111-120.

Huang, J., Xu, G., Hu, G., Kizil, M., & Chen, Z. (2018). A coupled electromagnetic irradiation, heat and mass transfer model for microwave heating and its numerical simulation on coal. *Fuel Processing Technology, 177*, 237-245.

Huang, Y. (2013). *Impact of Banana (Musa acuminata) ripening on resistant and non-resistant starch using hot-air and microwave drying* (Master's Thesis). McGill University, Quebec, Canada.

Huang, Z., Chen, Y., & Wang, S. (2020). Numerical studies on the electromagnetic and thermal performances of radio frequency disinfestation treatments for dried apricots. *Postharvest Biology and Technology, 163*, 111116.

Hui, L. Z. (2009). *Application of microwaves in pharmaceutical processes* (Doctoral dissertation). National University of Singapore, Singapore, Singapore.

Ikediala, J., Tang, J., Neven, L., & Drake, S. (1999). Quarantine treatment of cherries using 915 MHz microwaves: temperature mapping, codling moth mortality and fruit quality. *Postharvest Biology and Technology, 16*(2), 127-137.

Jain, D., Tang, J., Pedrow, P. D., Tang, Z., Sablani, S., & Hong, Y.-K. (2019). Effect of changes in salt content and food thickness on electromagnetic heating of rice, mashed potatoes and peas in 915 MHz single mode microwave cavity. *Food Research International, 119*, 584-595.

Jaiturong, P., Laosirisathian, N., Sirithunyalug, B., Eitssayeam, S., Sirilun, S., Chaiyana, W., & Sirithunyalug, J. (2020a). Physicochemical and prebiotic properties of resistant starch from *Musa sapientum* Linn., ABB group, cv. Kluai Namwa Luang. *Heliyon, 6*(12), e05789.

Jaiturong, P., Laosirisathian, N., Sirithunyalug, B., Eitssayeam, S., Sirilun, S., Chaiyana, W., & Sirithunyalug, J. (2020b). Potential of Musa sapientum Linn. for digestive function promotion by supporting Lactobacillus sp. *Heliyon, 6*(10), e05247.

John, P., & Marchal, J. (1995). Ripening and biochemistry of the fruit. In Gowen S. (Eds), *Bananas and plantains* (pp. 434-467). Dordrecht: Springer.

Jones, D., & Brischke, C. (2017). Chapter 10 - Modelling. In D. Jones, & C. Brischke (Eds.), *Performance of bio-based building materials* (pp. 483-546). Cambridge: Woodhead Publishing.

Ju, Y., Zhu, Y., Zhou, H., Ge, S., & Xie, H. (2021). Microwave pyrolysis and its applications to the in situ recovery and conversion of oil from tar-rich coal: An overview on fundamentals, methods, and challenges. *Energy Reports, 7*, 523-536.

Kampffmeyer, M. C. (2014). *Numerical modeling of microwave interactions with sea ice* (Master's Thesis). UiT The Arctic University of Norway, Tromsø, Norway.

Karim, M. A., & Hawlader, M. (2005). Drying characteristics of banana: theoretical modelling and experimental validation. *Journal of Food Engineering, 70*(1), 35-45.

Kaviany, M. (2012). *Principles of heat transfer in porous media*: Springer Science & Business Media.

Kelen, A., Ress, S., Nagy, T., Pallai, E., & Pintye-Hodi, K. (2006). Mapping of temperature distribution in pharmaceutical microwave vacuum drying. *Powder Technology, 162*(2), 133-137.

Khan, M. I. H., Joardder, M., Kumar, C., & Karim, M. (2018). Multiphase porous media modelling: A novel approach to predicting food processing performance. *Critical Reviews in Food Science and Nutrition, 58*(4), 528-546.

Khan, M. I. H., Welsh, Z., Gu, Y., Karim, M., & Bhandari, B. (2020). Modelling of simultaneous heat and mass transfer considering the spatial distribution of air velocity during intermittent microwave convective drying. *International Journal of Heat and Mass Transfer, 153*, 119668.

Kramer, A., & Twigg, B. A. (1962). Chapter 7 - Kinesthetics or texture. In A. Kramer, & B. A. Twigg (Eds.), *Fundamentals of quality control for the food industry* (pp. 83-105). Connecticut: AVI Publishing.

Kumar, C., Joardder, M., Farrell, T. W., & Karim, M. (2016). Multiphase porous media model for intermittent microwave convective drying (IMCD) of food. *International Journal of Thermal Sciences, 104*, 304-314.

Kumar, C., Joardder, M. U. H., Farrell, T. W., Millar, G. J., & Karim, A. (2018). A porous media transport model for apple drying. *Biosystems Engineering, 176*, 12-25.

Kumar, C., Joardder, M. U. H., Karim, A., Millar, G. J., & Amin, Z. (2014). Temperature redistribution modelling during intermittent microwave convective heating. *Procedia Engineering, 90*, 544-549.

Lahav, E. (1995). Banana nutrition. In S. Gowen (Ed.), *Bananas and plantains* (pp. 258-316). Dordrecht: Springer.

Larson, M. (2005). Numerical Modeling. In M. L. Schwartz (Ed.), *Encyclopedia of Coastal Science* (pp. 730-733). Dordrecht: Springer.

Lei, Z., Rougier, E., Euser, B., & Munjiza, A. (2020). A smooth contact algorithm for the combined finite discrete element method. *Computational Particle Mechanics, 7,* 807–821.

Lentzou, D., Boudouvis, A. G., Karathanos, V. T., & Xanthopoulos, G. (2019). A moving boundary model for fruit isothermal drying and shrinkage: An optimization method for water diffusivity and peel resistance estimation. *Journal of Food Engineering, 263*, 299-310.

Li, H., Shi, S., Lin, B., Lu, J., Lu, Y., Ye, Q., Wang, Z., Hong, Y., & Zhu, X. (2019). A fully coupled electromagnetic, heat transfer and multiphase porous media model for microwave heating of coal. *Fuel Processing Technology, 189*, 49-61.

Li, H., Zheng, C., Lu, J., Tian, L., Lu, Y., Ye, Q., Luo, W., & Zhu, X. (2019). Drying kinetics of coal under microwave irradiation based on a coupled electromagnetic, heat transfer and multiphase porous media model. *Fuel, 256*, 115966.

Liew, C., & Lau, C. (2012). Determination of quality parameters in Cavendish banana during ripening by NIR spectroscopy. *International Food Research Journal, 19*(2), 751.

Liu, G.-R., & Quek, S. S. (2013). Chapter 12 - FEM for Heat Transfer Problems. In G.R. Liu, & S.S. Quek (Eds.), *The finite element method: a practical course* (pp. 347-396). Oxford: Butterworth-Heinemann.

Liu, S., Fukuoka, M., & Sakai, N. (2013). A finite element model for simulating temperature distributions in rotating food during microwave heating. *Journal of Food Engineering, 115*(1), 49-62.

Liu, S., Ogiwara, Y., Fukuoka, M., & Sakai, N. (2014). Investigation and modeling of temperature changes in food heated in a flatbed microwave oven. *Journal of Food Engineering, 131*, 142-153.

Lo, S. (2002). Finite element mesh generation and adaptive meshing. *Progress in Structural Engineering and Materials, 4*(4), 381-399.

Logan, D. L. (2016). Chapter 1 - Introduction. In D. L. Logan (Ed.), *A first course in the finite element method* (pp. 1-30). Boston: Cengage Learning.

Malafronte, L., Lamberti, G., Barba, A. A., Raaholt, B., Holtz, E., & Ahrné, L. (2012). Combined convective and microwave assisted drying: Experiments and modeling. *Journal of Food Engineering, 112*(4), 304-312.

Marriott, J., Robinson, M., & Karikari, S. K. (1981). Starch and sugar transformation during the ripening of plantains and bananas. *Journal of the Science of Food and Agriculture, 32*(10), 1021-1026.

Martins, R. (2006). Simple finite volumes and finite elements procedures for food quality and safety simulations. *Journal of Food Engineering, 73*(4), 327-338.

Maskan, M. (2000). Microwave/air and microwave finish drying of banana. *Journal of Food Engineering, 44*(2), 71-78.

Mercier, S., Marcos, B., Moresoli, C., Mondor, M., & Villeneuve, S. (2014). Modeling of internal moisture transport during durum wheat pasta drying. *Journal of Food Engineering, 124,* 19-27.

Monteiro, R. L., Carciofi, B. A., & Laurindo, J. B. (2016). A microwave multi-flash drying process for producing crispy bananas. *Journal of Food Engineering, 178,* 1-11.

Mousa, N., & Farid, M. (2002). Microwave vacuum drying of banana slices. *Drying Technology, 20*(10), 2055-2066.

Naghavi, E.-A., Dehghannya, J., & Ghanbarzadeh, B. (2018). 3D computational simulation for the prediction of coupled momentum, heat and mass transfer during deep-fat frying of potato strips coated with different concentrations of alginate. *Journal of Food Engineering, 235,* 64-78.

Ni, H. (1997). *Multiphase moisture transport in porous media under intensive microwave heating* (Doctoral dissertation). Cornell University, New York, United States.

Ni, H., Datta, A., & Torrance, K. (1999). Moisture transport in intensive microwave heating of biomaterials: a multiphase porous media model. *International Journal of Heat and Mass Transfer, 42*(8), 1501-1512.

Onwude, D. I., Hashim, N., Abdan, K., Janius, R., & Chen, G. (2019). Experimental studies and mathematical simulation of intermittent infrared and convective drying of sweet potato (Ipomoea batatas L.). *Food and Bioproducts Processing, 114,* 163-174.

Pakdee, W., & Rattanadecho, P. (2011). Natural convection in a saturated variable-porosity medium due to microwave heating. *Journal of Heat Transfer, 133*(6), 062502.

Pandit, R., & Prasad, S. (2003). Finite element analysis of microwave heating of potato—transient temperature profiles. *Journal of Food Engineering, 60*(2), 193-202.

Panyakham, T., Panyakham, P., Chaiyasin, P., Oupkaew, P., Wangtueai, S., Charoenphun, N., & Lanoi, D. (2014). *Food product development from pisang awak (Musa sapientum L.) for Tapprik subdistrist administrative organization women group in Aranyaprathet district Sa-Kaeo province*. Chonburi: Burapha University.

Pillay, M., Tenkouano, A., Ude, G., & Ortiz, R. (2004). *Molecular characterization of genomes in Musa and its applications.* Paper presented at the Banana improvement: cellular, molecular biology, and induced mutations, Leuven, Belgium.

Pisutpaisal, N., Boonyawanich, S., & Saowaluck, H. (2014). Feasibility of biomethane production from banana peel. *Energy Procedia, 50,* 782-788.

Pitchai, K., Chen, J., Birla, S., Gonzalez, R., Jones, D., & Subbiah, J. (2014). A microwave heat transfer model for a rotating multi-component meal in a domestic oven: development and validation. *Journal of Food Engineering, 128,* 60-71.

Pragati, S., Genitha, I., & Ravish, K. (2014). Comparative study of ripe and unripe banana flour during storage. *Journal of Food Processing & Technology, 5*(11), 1-6.

Purlis, E. (2019). Modelling convective drying of foods: A multiphase porous media model considering heat of sorption. *Journal of Food Engineering, 263,* 132-146.

Rakesh, V., Datta, A. K., Walton, J. H., McCarthy, K. L., & McCarthy, M. J. (2012). Microwave combination heating: Coupled electromagnetics‐multiphase porous media modeling and MRI experimentation. *AIChE Journal, 58*(4), 1262-1278.

Ranjan, R., Irudayaraj, J., Reddy, J., & Mujumdar, A. (2004). Finite-element simulation and validation of stepwise drying of bananas. *Numerical Heat Transfer, Part A, 45*(10), 997-1012.

Ratanadecho, P., Aoki, K., & Akahori, M. (2002). Influence of irradiation time, particle sizes, and initial moisture content during microwave drying of multi-layered capillary porous materials. *Journal Heat Transfer, 124*(1), 151-161.

Raynolds, L. T. (2003). The global banana trade. In S. Striffler, & M. Moberg (Eds.), *Banana Wars: Power, Production, and History in the Americas* (pp. 23-47). London: Duke University Press.

Renshaw, R. C., Dimitrakis, G. A., & Robinson, J. P. (2021). Mathematical modelling of dielectric properties of food with respect to moisture content using adapted water activity equations. *Journal of Food Engineering, 300,* 110538.

Resurreccion Jr, F., Tang, J., Pedrow, P., Cavalieri, R., Liu, F., & Tang, Z. (2013). Development of a computer simulation model for processing food in a microwave assisted thermal sterilization (MATS) system. *Journal of Food Engineering, 118*(4), 406-416.

Roohi, R., & Hashemi, S. M. B. (2020). Experimental, heat transfer and microbial inactivation modeling of microwave pasteurization of carrot slices as an efficient and clean process. *Food and Bioproducts Processing, 121,* 113-122.

Ruben, R., & van Schendel, L. (2008). Impact of Fairtrade in banana plantations in Ghana: Income, ownership and livelihoods of banana workers. In R. Ruben (Ed.), *The Impact of Fairtrade* (pp. 137-154). Wageningen: Wageningen Academic Publishers.

Ryynänen, S. (2002). *Microwave heating uniformity of multicomponent prepared foods* (Doctoral dissertation). University of Helsinki, Helsinki, Finland.

Salvi, D., Boldor, D., Aita, G., & Sabliov, C. (2011). COMSOL Multiphysics model for continuous flow microwave heating of liquids. *Journal of Food Engineering, 104*(3), 422-429.

Selimefendigil, F., Çoban, S. Ö., & Öztop, H. F. (2021). Investigation of time dependent heat and mass transportation for drying of 3D porous moist objects in convective conditions. *International Journal of Thermal Sciences, 162,* 106788.

Seymour, G. B. (1993). Chapter 3 - Banana. In G.B. Seymour, J.E. Taylor, & G. A. Tucker (Eds.), *Biochemistry of fruit ripening* (pp. 83-106). Dordrecht: Springer.

Shabana, A. A. (2018). Chapter 7 - Computational Geometry and Finite Element Analysis. In A. A. Shabana (Ed.), *Computational Continuum Mechanics* (pp. 261-277). New Jersey: Wiley.

SHARP. (2013). *Microwave Oven R-299 Operation Manual*. Bangkok: Sharp Thai Co., Ltd.

Shen, L., Zhu, Y., Liu, C., Wang, L., Liu, H., Kamruzzaman, M., Liu, C., Zhang, Y., & Zheng, X. (2020). Modelling of moving drying process and analysis of drying characteristics for germinated brown rice under continuous microwave drying. *Biosystems Engineering, 195,* 64-88.

Siriboon, N., & Banlusilp, P. (2004). A study on the ripening process of 'Namwa'banana. *AU Journal of Technology, 7*(4), 159-164.

Sirois, F., & Grilli, F. (2015). Potential and limits of numerical modelling for supporting the development of HTS devices. *Superconductor Science and Technology, 28*(4), 043002.

Smith, N., Seymour, G., Jeger, M., & Tucker, G. (1990). Cell wall changes in bananas and plantains. *Acta Horticulturae. 269,* 283-290.

Soltani, M., Alimardani, R., Omid, M., & Karaj, I. (2011). Changes in physico-mechanical properties of banana fruit during ripening treatment. *Journal of American Science, 7*(5), 14-19.

Song, C., Wu, T., Li, Z., Li, J., & Chen, H. (2018). Analysis of the heat transfer characteristics of blackberries during microwave vacuum heating. *Journal of Food Engineering, 223,* 70-78.

Stover, R. H., & Simmonds, N. W. (1987). Chapter 18 - Fruit physiology, biochemistry and nutritional values. In R. H. Stover, & N. W. Simmonds (Eds.), *Bananas* (pp. 386-390). Essex: Longman Scientific & Technical.

Sun, X., Schmidt, S. J., & Litchfield, J. B. (1994). Temperature mapping in a potato using half Fourier transform MRI of diffusion. *Journal of Food Process Engineering, 17*(4), 423-437.

Suwannapum, N., & Rattanadecho, P. (2011). Analysis of heat–mass transport and pressure buildup induced inside unsaturated porous media subjected to microwave energy using a single (TE_{10}) mode cavity. *Drying Technology, 29*(9), 1010-1024.

Swasdisevi, T., Devahastin, S., Ngamchum, R., & Soponronnarit, S. (2007). Optimization of a drying process using infrared-vacuum drying of Cavendish banana slices. *Optimization, 29*(3), 810.

Thaiphanit, S., & Anprung, P. (2010). Physicochemical and flavor changes of fragrant banana (*Musa acuminata* AAA group "Gross Michel") during ripening. *Journal of Food Processing and Preservation, 34*(3), 366-382.

Thorvaldsson, K., & Janestad, H. (1999). A model for simultaneous heat, water and vapour diffusion. *Journal of Food Engineering, 40*(3), 167-172.

Udomdetwatthana, S. (1993). *Thermal properties of Musa suerier and Musa sapientum Linn* (Master's Thesis). Chulalongkorn University, Bangkok, Thailand.

Upadhyay, S., & Rai, K. N. (2019). A new iterative least square Chebyshev wavelet Galerkin FEM applied to dual phase lag model on microwave drying of foods. *International Journal of Thermal Sciences, 139,* 217-231.

USDA (2004). *Bananas-Market Inspection Instructions*. Washington DC: USDA Agricultural Marketing Service.

Van Groesen, E., & Molenaar, J. (2007). Chapter 1 - Dimensional Analysis and Scaling. In E. Van Groesen, & J. Molenaar (Eds.), *Continuum modeling in the physical sciences* (pp. 1-30). Philadelphia: SIAM.

Vatanasuchart, N., Butsuwan, P., & Narasri, W. (2015). Nutritional composition, in vitro starch digestibility and estimated glycemic index of three varieties of'Kluai Namwa'banana (Musa sapientum L.) and its products. *Maejo International Journal of Science and Technology, 9*(2), 265-277.

Vatanasuchart, N., Niyomwit, B., & Narasri, W. (2012). Resistant starch, physicochemical and structural properties of bananas from different cultivars with an effect of ripening and processing. *Agriculture and Natural Resources, 46*(3), 461-472.

Venkatesh, M., & Raghavan, G. (2004). An overview of microwave processing and dielectric properties of agri-food materials. *Biosystems Engineering, 88*(1), 1-18.

Wai, C., Rivai, A., & Bapokutty, O. (2013). *Modelling optimization involving different types of elements in finite element analysis.* IOP Conference Series: Materials Science and Engineering, *50,* 012036. Paper presented at the 2nd International Conference on Mechanical Engineering Research (ICMER 2013), Pahang, Malaysia.

Wainwright, H., & Hughes, P. (1990). Changes in banana pulp colour during ripening. *Fruits, 45*(1), 25-28.

Wills, R., & Golding, J. (2016). Chapter 1 - Introduction. In R. Wills, & J. Golding (Eds.), *Postharvest: an introduction to the physiology and handling of fruit and vegetables* (pp. 1-15). Sydney: UNSW press.

Ye, J., Xu, C., Zhang, C., Zhu, H., Huang, K., Li, Q., Wang, J., Zhou, L., & Wu, Y. (2021). A hybrid ALE/implicit function method for simulating microwave heating with rotating objects of arbitrary shape. *Journal of Food Engineering, 302,* 110551.

Ye, X., Ruan, R., Chen, P., & Doona, C. (2004). Simulation and verification of ohmic heating in static heater using MRI temperature mapping. *LWT-Food Science and Technology, 37*(1), 49-58.

Yi, Q., Lan, J., Ye, J., Zhu, H., Yang, Y., Wu, Y., & Huang, K. (2021). A simulation method of coupled model for a microwave heating process with multiple moving elements. *Chemical Engineering Science, 231,* 116339.

Youryon, P., & Supapvanich, S. (2016). Quality and bioactive compounds of ripe'Kluai Nam Wa'and'Kluai Khai'bananas during storage. *International Food Research Journal, 23*(3), 1027-1032.

Youryon, P., & Supapvanich, S. (2017). Physicochemical quality and antioxidant changes in 'Leb Mue Nang'banana fruit during ripening. *Agriculture and Natural Resources, 51*(1), 47-52.

Zhang, Y. J. (2018). Chapter 4 - Fundamentals to Geometric Modeling and Meshing. In Y. J. Zhang (Ed.), *Geometric modeling and mesh generation from scanned images* (pp. 99-154). New York: CRC Press.

Zhang, Z., Su, T., & Zhang, S. (2018). Shape effect on the temperature field during microwave heating process. *Journal of Food Quality,* 1-24.

Zhou, J., Yang, X., Chu, Y., Li, X., & Yuan, J. (2020). A novel algorithm approach for rapid simulated microwave heating of food moving on a conveyor belt. *Journal of Food Engineering, 282,* 110029.

Zhu, H., He, J., Hong, T., Yang, Q., Wu, Y., Yang, Y., & Huang, K. (2018). A rotary radiation structure for microwave heating uniformity improvement. *Applied thermal engineering, 141,* 648-658.

Zotarelli, M. F., Porciuncula, B. D. A., & Laurindo, J. B. (2012). A convective multi-flash drying process for producing dehydrated crispy fruits. *Journal of Food Engineering, 108*(4), 523-531.

APPENDIX

Appendix A1: The single-phase simulation model of temperature profiles with photos of banana samples used in the experiments at over time; (a) unripe banana; (b) ripe banana.

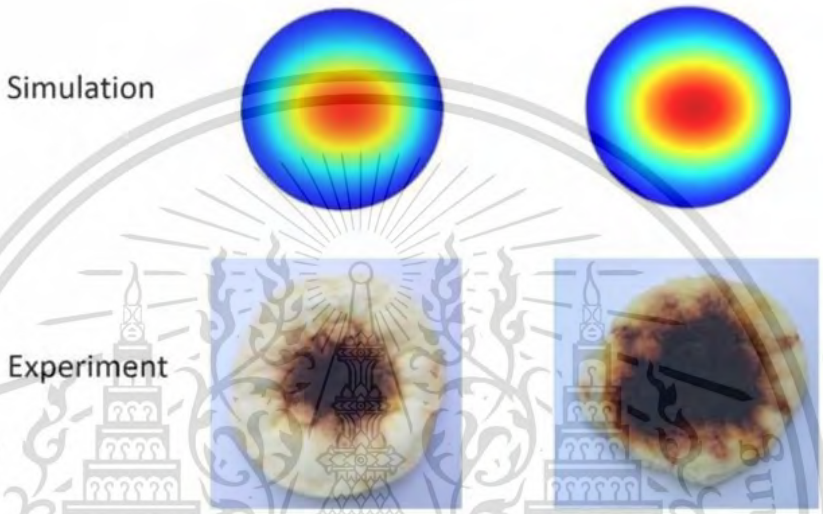

Appendix A2: The single-phase simulation model of temperature profiles with photos of banana samples used in the experiments at over time; (a) transversal; (b) longitudinal.

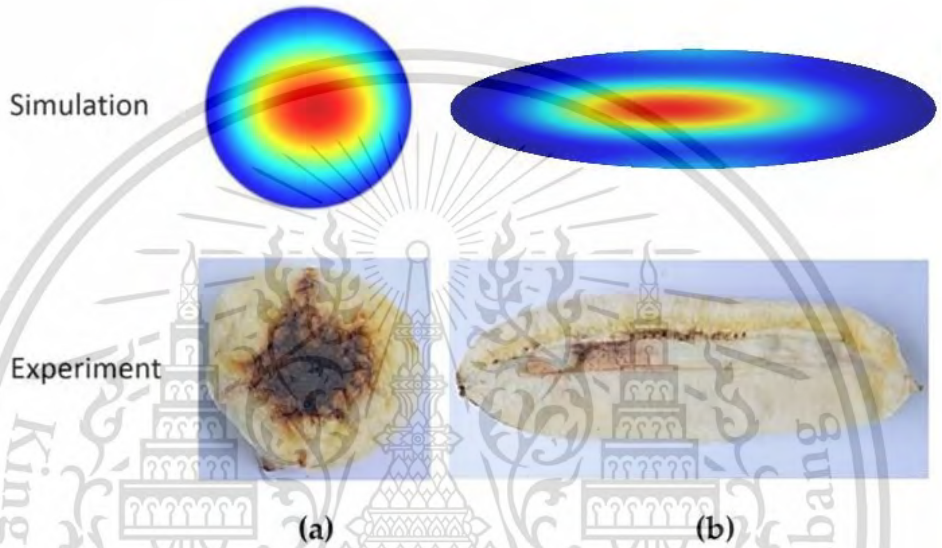

Appendix A3: Comparison of: (a) the multi-phase porous media simulation model of temperature profiles with (b) infrared thermal images and (c) photos of unripe banana samples used in the experiments at different time intervals.

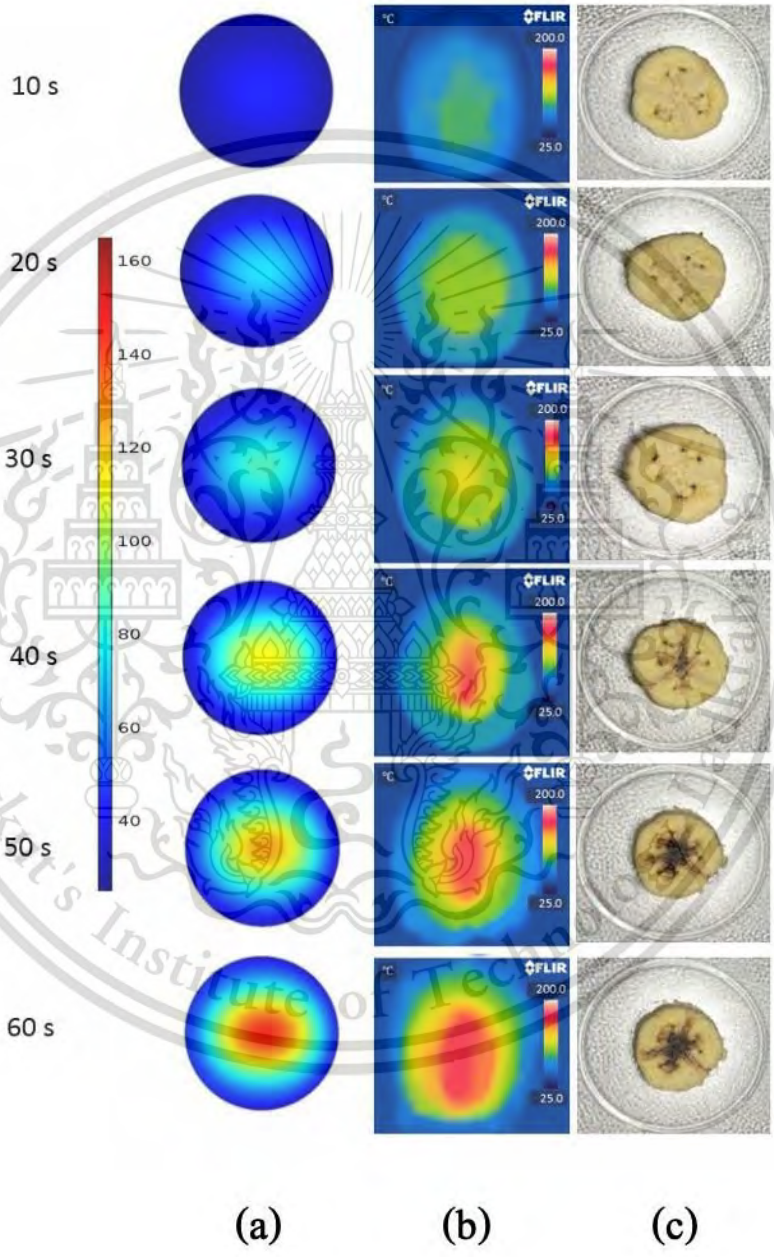

Appendix A4: Comparison of: (a) the multi-phase porous media simulation model of temperature profiles with (b) infrared thermal images and (c) photos of ripe banana samples used in the experiments at different time intervals.

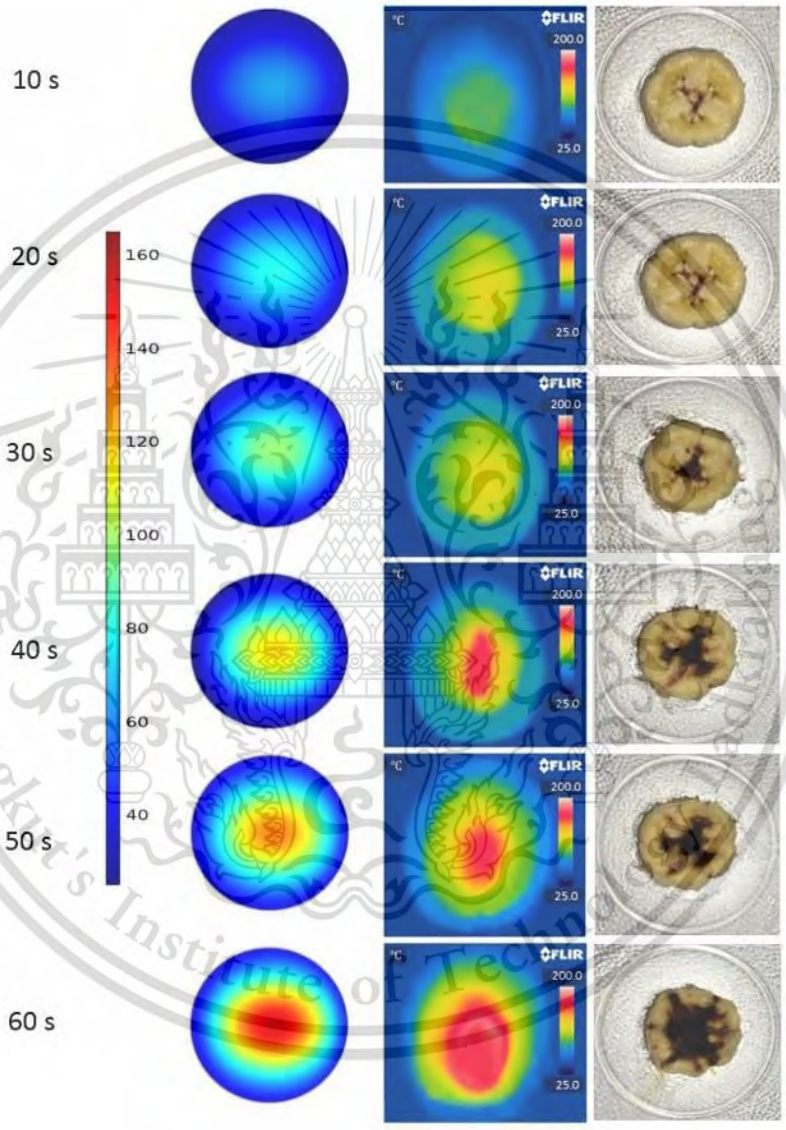

AUTHOR BIOGRAPHY

Name Miss Wisara Thuto

Educations

- B.Sc. (Food Science and Technology), Rajamangala University of Technology Tawan-Ok (Bangpra Campus).
- M.Sc. (Food Science), King Mongkut's Institute of Technology Ladkrabang.
- Ph.D. (Food Science, International Program), King Mongkut's Institute of Technology Ladkrabang.

Publications

- Thuto, W., & Banjong, K. (2015). *Modeling the microwave heat distribution of banana at different ripening stages.* Paper presented at the 2nd International Symposium on Agricultural Technology (ISAT2015), Pattaya, Thailand.
- Thuto, W., & Banjong, K. (2015). Temperature Profile Prediction on Three Shapes of Banana Slices During Microwave Heating. *Int. Proc. Chem. Biol. Environ. Eng., 86*, 42-48.
- Thuto, W., & Banjong, K. (2019). Investigation of Heat and Moisture Transport in Bananas during Microwave Heating Process. *Processes, 7*(8), 545.
- Thuto, W., & Banjong, K. (2021). *Computational Modeling of Microwave Dehydration of Unripe and Ripe Bananas Considering Shrinkage.* Paper presented at the 7th International Conference on Food and Agricultural Engineering (ICFAE 2021), Virtual conference.
- Thuto, W., & Banjong, K. (2021). *Prediction of airflow pattern and temperature profiles Inside microwave oven during banana dehydration process*. Paper presented at the 7th International Conference on Food and Agricultural Engineering (ICFAE 2021), Virtual conference.